Available online www.jocpr.com

Journal of Chemical and Pharmaceutical Research, 2016, 8(1):639-662

Research Article

ISSN : 0975-7384
CODEN(USA) : JCPRC5

Synthesis, spectral characterization and thermal analysis of some alloxan, carmine, naphthol yellow S and hematoxylin complexes

Mamdouh S. Masoud[a], Rabah H. A. Mohamed[a], Alaa E. Ali[b*] and Najat O. M. EL-Ziani[c]

[a]*Chemistry Department, Faculty of Science, Alexandria University, Alexandria, Egypt*
[b]*Chemistry Department, Faculty of Science, Damanhour University, Damanhour, Egypt*
[c]*Chemistry Department, Faculty of Science, Sirt University, Sirt, Libya*

ABSTRACT

Syntheses of alloxan, carmine, naphthol yellow S and hematoxylin complexes have been reported. Elemental analysis of the prepared metal complexes, structural investigation of the complexes to know their geometries and mode of bonding based on: Infrared, electronic spectra and magnetic susceptibility, ESR study of copper complexes were studied. Some theoretical studies were carried out to obtain the charges, bond length, bond angles, and dihedral angles of the studied ligands, where the chemical potential, electronegativity, hardness and softness are determined, using hyperchem program. All the iron, cobalt and nickel complexes are with octahedral geometry, except Co-alloxan complex is with Td geometry. However, the copper and cadmium alloxan complexes are with square planner geometry. The thermal properties of the studied complexes were examined. Molecular modeling of the ligands was performed using PC computer to give extra spot lights on the bonding properties of these compounds.

Keywords: Alloxan, Carmine, Naphthol Yellow S, Hematoxylin, complexes, spectral investigation, thermal analysis.

INTRODUCTION

Alloxan drivatives are widely used to induce experimental diabetes in animals and the action mechanism in β cells of the pancreas has been investigated [1,2]. It inhibits pro-insulin synthesis in pancreatic islets [3]. Alloxan is a strong oxidizing agent and it forms a hemiacetal with its reduced reaction product dialuric acid (in which a carbonyl group is reduced to a hydroxyl group) which is called alloxantin [4]. They establish a redox cycle with the formation of superoxide radicals which undergo dismutation to hydrogen peroxide. Thereafter highly reactive hydroxyl radicals are formed by the Fenton reaction [1,2].

Alloxan is an alter dentate ligand offering more than one equivalent coordination site, where always a rearrangement is possible in which the metal is transferred from one site to another. This can be either an inter- or intramolecular process. The rearrangement is kinetically controlled by the activation energy and entropy on the reaction path. The free energy difference is zero by definition if the coordination sites are equivalent [5,6]. Alloxan can coordinate with several types of structures [7,8]. Purity and morphology of the complexes obtained were studied by SEM. The obtained SEM micrographs allow verifying that the complexes are well formed amorphous shapes[9].

Naphthol yellow S (flavianic acid disodium salt) is used as yellow colorant for cosmetics of dyeing hair, can decompose and burn spontaneously in the producing process. The prediction results by the Computer Program for Chemical Thermodynamic and Energy Release Evaluation (CHETAH) suggest flavianic acid hydrate (the former production of flavianic acid disodium salt) and flavianic acid disodium salt have high rank of maximum heat of decomposition and fuel value-heat of decomposition. The rank of explosive hazard for flavianic acid disodium salt was II by the Differential Scanning Calorimetry (DSC) and Pressure Vessel Test (PVT) according to the evaluation method in the Japanese Fire Service Law. The Accelerating Rate Calorimeter (ARC) demonstrates particle size difference that has no significant effect on the thermal stability of flavianic acid disodium salt. Compared with flavianic acid, disodium salt, flavianic acid hydrate had low thermal stability [10].

Hematoxylin stains has been used for at least a century and are still essential for recognizing various tissue types and the morphologic changes that form the basis of contemporary cancer diagnosis. Hematoxylin has a deep blue-purple color and stains nucleic acids by a complex, incompletely understood reaction. In a typical tissue, nuclei are stained blue, whereas the cytoplasm and extracellular matrix have varying degrees of pink staining. Well-fixed cells show considerable intranuclear detail. Nuclei show varying cell-type- and cancer-type-specific patterns of condensation of heterochromatin (hematoxylin staining) that are diagnostically very important. If abundant polyribosomes are present, the cytoplasm will have a distinct blue cast. The Golgi zone can be tentatively identified by the absence of staining in a region next to the nucleus. Thus, the stain discloses abundant structural information, with specific functional implications. A limitation of hematoxylin staining is that it is incompatible with immunofluorescence. It is useful, however, to stain one serial paraffin section from a tissue in which immunofluorescence will be performed. Hematoxylin is useful as a counterstain for many immune histochemical or hybridization procedures that use colorimetric substrates [11]. Photoswitchable fluorescent probes have been used in recent years to enable super-resolution fluorescence microscopy by single molecule imaging [12-14]. In our laboratory, Masoud*et al studied* the chemistry of nucleic acid constituents and their complexes [15-21]. The structures of the studied organic compounds are represented in Figure 1.

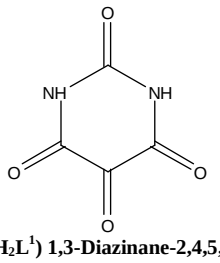

Alloxan (H_2L^1) 1,3-Diazinane-2,4,5,6-tetrone

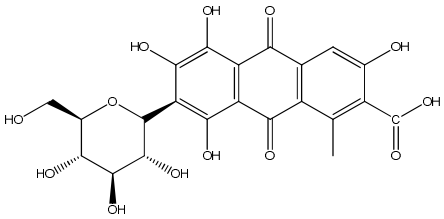

carmine (H_9L^2) 7-beta-D-glucopyranosyl-3,5,6,8-tetrahydroxy-1-methyl-9,10-dioxo-anthracene-2-carboxylic acid

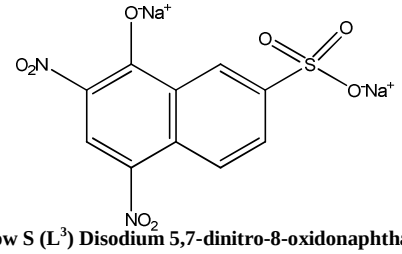

naphthol yellow S (L^3) Disodium 5,7-dinitro-8-oxidonaphthalene-2-sulfonate

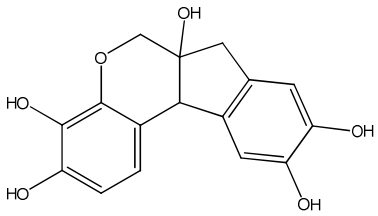

hematoxylin (H_5L^4) 7,11b-Dihydroindeno[2,1-c]chromene-3,4,6a,9,10(6H)-pentol

Figure 1. The structures of the studied ligands

EXPERIMENTAL SECTION

Ligands:
The selected ligands [Alloxan (H_2L^1), Carmine (H_9L^2), Naphthol Yellow S (L^3) and Hematoxylin (H_5L^4)], and starting materials used in this work were obtained from Fluka, Sigma and Lobachemie companies and used without further purification.

Complexes:
All the complexes either simple or mixed were prepared in a similar manner. The required weight of transition metal chloride salt (Fe, Co, Ni, Cu, Cd) and the ligand were dissolved in different solvents (methanol, DMF, ethanol). The transition metal chloride solution was mixed with that of the ligand. The reaction mixture was refluxed for 5min, then cooled where a precipitate was formed, filtered then dried in an oven at ~ 90^{o}C. The products were analyzed to be 1:1, 2:1 and 2:3 (M:L) molar ratio for simple complexes, while those of the mixed are with molar ratio 1:1:2 , 1:1:1 (M:M`:L)and 1:1:1**:1** (M:M`:M``:L). All complexes are with melting points higher than 300^{o}C. However, all complexes were prepared in presence of ammonia except iron complexes. All solvents were of spectroquality grade and were used without purification.

Instruments and working procedures:
The metal contents were determined by atomic absorption technique at the central laboratory, Faculty of Science, Alexandria University. The metal contents were also determined titrimetrically with standard EDTA solution [22]. Carbon, Hydrogen, Nitrogen and Chloride contents were analyzed as usual. The infrared spectra of the ligands and their metal complexes were taken in KBr disc using Bruker -Tensor 37 (FT-IR system spectrum BX) covering a range from 400-4000 cm^{-1}. Calibration of frequency reading was made with polystyrene film. The spectral studies in solution were measured using Double beam uv- visible spectrophotometry (Jasco-V.530) and Perkin Elmer (Lambda 4B)covering the wavelength range 200-600nm and 190-900nm, respectively.

X-band electron spin resonance spectra were recorded with JES- FE2XG- ESR Spectrometer (JEOL). The g-values were determined by comparison with DPPH (Diphenylpicrylhydrazide) signal. Molar conductivities of freshly prepared complexes (1X10^{-3}M) in DMSO and ethanol were measured using (HANNA-HI8033 conductivity).Molar magnetic susceptibility corrected for diamagnetism using Pascal's constant, were determined at room temperature (298°K) using Faraday's method. The apparatus was calibrated with $HgCo(SCN)_4$ [23]. The chem. office ultra 2002 and hyper chem. computer program has been used to generate molecular modeling of the compounds and their complexes. The physical properties and analytical data for the ligands and the prepared complexes are represented in Table 1.

Differential thermal analysis (DTA), thermogravimetric analysis (TG) and differential scanning calorimetry (DSC) were carried out using a LINSEIS STA PT 1000, TG- 50 Shimadzu and DSC- 60A Shimadzu. The rate of heating was 10 and 20^{o}C/min. The cell used was Platinum, the atmospheric nitrogen was flowed over the sample at a rate 20 cm3 min-1 and a chamber cooling water flow was 10 L^{-1} h^{-1}.

RESULTS AND DISCUSSION

Ir spectra of Alloxan and its complexes:

The fundamental infrared bands of alloxan and its complexes are given in Table (2). By comparing of the infrared spectrum of the complexes with that of free ligand, it should be possible to determine the binding sites. The vibrational frequencies of coordinated functional groups (e.g $\nu_{OH,}$ $\nu_{NH,\ \nu\ N=C-O)}$ are affected with different degrees.

a) The band at 3430 cm^{-1} in the free ligand, assigned as ν_{OH}, undergoes a strong shift within a range of 3431-3465cm^{-1}in all complexes except in the copper-nickel complex that is disappeared. Such region identifies also the presence of hydrogen bond.

b) Two bands at 3043 and 2809cm^{-1}, are assigned to ν_{NH} [24]. They are disappeared in all complexes, indicating that the chelation occurs at NH group.

c) The $\nu_{(C(2)=O)}$ and the overlapped $\nu_{\ (C(4)=O),}$ $\nu_{(C(6)=O)}$ of free ligand appeared at 1767and 1708cm^{-1}, respectively. The first band was assigned to the alloxan amide fragment (-NH-CO-NH-), and is disappeared in all complexes except in iron complex, where it splits to 1771 and 1762cm^{-1}. The overlapped $\nu_{(C(4)=O)}$, $\nu_{(C(6)=O)}$ band is appeared in all complexes with a red shift, except in iron and copper-cobalt complexes is absent. It was assigned to asymmetric and symmetric vibrations of two ketone groups in positions 4 and 6 [25].

Table (1) Physical properties and analytical data for compounds and the prepared complexes

Complex	M.wt	Formula	Calculated/ Found %						
			C%	H%	N%	M%			Cl%
Alloxan (H_2L^1)H_2O	160.09	$C_4H_2N_2O_4$-H_2O	-	-	-	-			-
[Fe(L^1)(H_2O)$_3$Cl]2H_2O	321.4	$C_4H_{10}N_2FeO_9Cl$	14.9 (15.2)	3.1 (3.3)	8.7 (9.1)	17.3 (17.6)			11.04 (11.12)
[Co(L^1)(H_2O)$_2$]3H_2O	289.02	$C_4H_{12}N_2CoO_9$	16.6 (16.8)	4.1 (4.0)	9.6 (9.9)	20.3 (19.8)			-
[Ni(L^1)(H_2O)$_4$]3H_2O	324.8	$C_4H_{14}N_2$ Ni O_{11}	14.6 (15.1)	4.3 (3.9)	8.6 (8.6)	18.0 (18.1)			-
[Cu(L^1)(H_2O)$_2$]H_2O	257.6	$C_4H_6N_2CuO_7$	18.6 (18.5)	2.3 (2.4)	10.8 (10.5)	24.6 (24.9)			-
[Cd(HL^1)H_2OCl]2H_2O	342.9	$C_4H_7N_2CdO_7Cl$	13.9 (14.3)	2.0 (2.5)	8.1 (8.3)	32.7 (32.5)			10.35 (10.72)
[CuCo(HL^1)(H_2O)$_3$OHCl_2]2H_2O	441.3	$C_4H_{12}N_2CuCoO_{10}Cl_2$	10.8 (10.6)	2.9 (3.4)	6.3 (6.4)	14.4 (14.2)	13.3 (13.2)		16.08 (16.45)
[CuNi(HL^1)$_2Cl_2$]5H_2O	583.4	$C_8H_{14}N_4CuNiO_{14}Cl_2$	16.4 (16.5)	9.5 (9.8)	9.5 (9.8)	10.8 (10.4)	10.1 (10.3)		12.17 (12.13)
[CuNiCo(HL^1)(NH_3)$_4Cl_4$]6H_2O	567.2	$C_4H_{26}N_6CuNiCoO_{11}$ Cl_4	7.3 (7.2)	12.7 (12.9)	12.7 (12.9)	9.6 (8.9)	8.9 (9.3)	8.9 (9.4)	21.60 (21.73)
Carmine (H_9L^2)	492.40	$C_{22}H_{20}O_{13}$	-	-	-	-			-
[Fe_2(H_7L^2)$_2$(H_5L^2)(H_2O)$_4$]6H_2O	1760.9	$C_{66}H_{72}$ Fe_2 O_{49}	44.9 (44.5)	4.1 (4.5)	-	6.3 (5.9)			-
[Co(H_7L^2)(H_2O)$_4$]	621.33	$C_{22}H_{26}CoO_{17}$	42.4 (42.7)	4.1 (4.5)	-	9.4 (9.4)			-
[Ni(H_7L^2)(H_2O)$_4$]2H_2O	657.11	$C_{22}H_{30}$ Ni O_{19}	40.1 (40.4)	4.6 (5.1)	-	8.9 (8.8)			-
[Cu(H_7L^2)(H_2O)$_2$]	589.95	$C_{22}H_{22}$ Cu O_{15}	44.7 (44.9)	3.7 (4.1)	-	10.7 (11.2)			-
Naphthol yellow S (L^3)	358.19	$C_{10}H_4N_2O_8SNa_2$	-	-	-	-			-
[Co_2(L^3)(H_2O)$_6Cl_2$]2H_2O	645.05	$C_{10}H_{20}N_2(Co)_2O_{16}SCl_2$	18.6 (18.5)	3.1 (3.4)	4.3 (4.1)	18.2 (17.8)			11.0 (11.3)
Hematoxylin (H_4L^5)3H_2O	356.28	$C_{16}H_{14}O_6$-3H_2O	-	-	-	-			-
[Fe(H_3L^4)(H_2O)$_3$Cl]4H_2O	517.63	$C_{16}H_{26}$ Fe $O_{13}Cl$	37.1 (37.1)	5.0 (5.1)	-	10.7 (10.3)			6.8 (7.2)
[Co(H_3L^4)(H_2O)$_4$]5H_2O	521.21	$C_{16}H_{30}CoO_{15}$	36.8 (36.4)	5.7 (6.1)	-	11.3 (11.4)			-
[Ni(H_3L^4)(H_2O)$_4$]5H_2O	520.99	$C_{16}H_{30}Ni$ O_{15}	36.8 (36.9)	5.7 (6.1)	-	11.2 (11.2)			-
[Cu(H_3L^4)(H_2O)$_2$]3H_2O	453.83	$C_{16}H_{22}$ Cu O_{11}	42.3 (42.4)	4.8 (5.1)	-	14.0 (13.5)			-

**The melting points for all complexes > 300^oC.*

d)$\nu_{N=C-O,}$ in all complexes exhibits one band at the range of 1622-1638cm^{-1}. However, Cu-Ni complex exhibits two bands at 1636 and 1541cm^{-1}.These bands are not detected in the free ligand, supporting the existence of the enol form during the complexation. Also, this is confirmed by the presence of ν_{OH} in the complexes.

e) The bands at 1451 and 1397cm^{1} identified for the ν_{NH} in free ligand. The second band is appeared in all complexes with a red shift at 1400cm^{-1}, whereas the first band is disappeared in all complexes except in Cu-Ni complex with a red shift at 1457cm^{-1}.

Table (2): Fundamental infrared bands of alloxan ($H_2L_1.H_2O$) and its complexes

Compound	ν_{OH}	ν_{NH}	$\nu_{(C(2)=O)}$	$\nu_{(C(4)=O)}$, $\nu_{(C(6)=O)}$	$\nu_{(N=CO)}$	δ_{NH}	δ_{OH}	$\nu_{C=O}$	ν_{C-N}	ν_{C-C}	$\delta_{C=O}$ δ_{NH}	ν_{M-O} ν_{M-N}
$H_2L_1H_2O$	3430	3043 2809	1767	1708	-	1451 1397	1365	1252	1170	1038 1021	807 781 766	-
$[Fe(L^1)(H_2O)_3Cl]2H_2O$	3437	-	1771 1762	-	1636	1400	-	1265	1162	-	-	526
$[Co(L^1)(H_2O)_3]3H_2O$	3433	-	-	1728	1633	1401	-	-	1153	1096	-	583
$[Ni(L^1)(H_2O)_4]3H_2O$	3431	-	-	1723	1622	1400	-	-	1161	1061	-	636
$[Cu(L^1)(H_2O)_2]H_2O$	3435	-	-	1737	1638	1401	-	-	1155	-	779	587 509
$[Cd(HL^1)H_2OCl]2H_2O$	3465	-	-	1725	1638	-	1359	1290	-	1066	783	524
$[CuNi(HL^1)_2Cl_2]5H_2O$	-	-	-	1717	1636 1541	1457	1351	-	-	-	-	617
$CuCo(HL^1)(H_2O)_3OH2Cl]\ 2H_2O$	3431	-	-	-	1632	1400	1365	1290	1154	-	782	587
$[CuNiCo\ (L^1)(NH_3)_4Cl_4]\ 6H_2O$	3436	-	-	1719	1636	1400	-	1293	1152	-	-	580

f) The band at 1365cm^{-1} is identified for the δ_{OH} in free alloxan. It undergoes strong shift within the range of 1351-1365cm^{-1} in mixed copper–nickel, copper-cobalt and cadmium complexes, while it is disappeared in the others. This indicates the presence of the keto –enol tautomers.

g) The band at 1252 cm^{-1} assigned to the ν_{C-O} [26] in the free ligand, undergoes a strong shift in the range of 1265-1293cm^{-1} in the iron, cadmium, copper-cobalt and copper-cobalt-nickel complexes, while it is disappeared in the others.

h) In the free ligand, ν_{CN}b and appeared at 1170cm^{-1}, is disappeared in cadmium and copper-nickel complexes, while in other complexes, it exhibits a strong shift within the range of 1152-1162cm^{-1}.

i) The ν_{C-C} 27]bands of alloxan appeared at 1021and 1038cm^{-1}, where the first band was absence in all complexes, and the second are observed only for Ni, Co, Cd complexes within the range of 1061-1096cm^{-1}.

j) Three bands at 766, 781, 807 cm^{-1} assigned to $\delta_{C=O}$ δ_{NH}, are disappeared in all complexes except 781 cm^{-1} band is shifted in Cu, Cd, Cu-Co complexes.

k) New intense bands appeared in all alloxan complexes in the frequency ranges 509-636 cm^{-1}, are attributed to overlap the bands of ν_{M-O} and ν_{M-N}.

The different modes of vibrations of the C=O and N-H groups leading to assume that the hydrogen bonding is a major importance. The separation in frequency for each group (e.g. carbonyl) reveals that the carbonyl groups exhibit different bond order. One of the carbonyl groups is polarized under the influence of the intramolecular charge transfer effect leading to a band with lower wave number while the second is not charged leading to another band at wavenumber, depending on the coupling between the characteristic vibrations of the carbonyl groups.

IR spectra of Carmine and its complexes:

The infrared spectral data for carmine and its metal complexes, Table (3), gave the following:

a) One broad band appeared for carmine ligand at 3430cm^{-1}, is assigned due to ν_{OH} 28,29], and appeared in all complexes, within strong shift in the range of 3408-3447cm^{-1}. This indicated the interaction between the metal and the OH groups.

b) The ν_{CH} band appeared in carmine free ligand and its iron complex at 2928 and 2929cm^{-1}, respectively. But in the other complexes, the band is absent.

c) Three bands at 1638, 1570 and 1470cm^{-1} are assigned to$\nu_{C=C}\nu_{C-C}$ in free ligand. The first two bands in all complexes are shifted within the range of 1636-1653cm^{-1} and 1564-1568cm^{-1}, respectively, while the third are absent in all the complexes.

d)The carmine ligand gave only one band at 1412cm^{-1}, assigned to $\nu_{COO}\delta_{OH}$. This band is split into two bands in the other complexes. This band is appeared in the range of 1401-1420cm^{-1}in all complexes, but in Fe-complex, it is strongly blue shifted to 1392cm^{-1}.Anew band is present in the Co, Ni and Fe complexes at higher frequencies within the range of 1313-1340cm^{-1}. So, the OH group is affected on complexation or due to the existence of water molecule.

e) The ν_{OH} bands appeared at 896 and 771cm^{-1} in carmine, while they are detected in Cu- and Fe-complexes at (895,778cm^{-1}) and (896, 853, 772cm^{-1}), respectively. But in cobalt- and nickel-complexes, these bands are disappeared.

f) The $\delta_{C=O}$ bands in free ligand are observed at 667 and 616cm^{-1}. The two bands appeared in all complexes except in Cu and Co complexes. The first band is unchanged, but the second is shifted within the range of 603-607cm^{-1}.

g)The ν_{CO} in the carmine is observed at 544 and 457cm^{-1}. The first band is shifted in case of the nickel complex and disappeared in the other complexes. The second band is detected only in iron complex.

h)The different modes of vibrations of C-C, C=C and CH are affected on complexation, probably due to that the aromaticity of the formed chelate differs from that of the ligand.

i) New bands are appeared in all carmine complexes in frequency ranges 470-608cm^{-1}, attributed to ν_{M-O}.

IR spectra of Naphthol yellow S and its complex:

The infrared spectra of naphthol yellow S and its complexes, Table (4), pointed to the vibrational frequencies of coordinated functional group (e.g. ν_{SO3}^{-},ν_{NO2}, ν_{S-O},ν_{C-N}) are affected with different degrees.

a) The ν_{OH} band is assigned at 3432cm^{-1}, while in the corresponding cobalt-complex it becomes at 3436cm^{-1}. The band at 3432cm^{-1} in free ligand attributed to adsorbed water.

b)The intense bands at 1195, 1166 and 1148cm^{-1} in free ligand are assigned to the ν_{SO}^{-3}. They are present in its cobalt complex, but the third band is absent.

Table (3): Fundamental infrared bands of carmine (H_9L^2) and its complexes

Compound	ν_{OH}	ν_{CH}	$\nu_{C=C}$ ν_{C-C}	ν_{C-OO} δ_{OH}	ν_{C-OH}	ν_{OH}	$\nu_{C=O}$	ν_{CO}	ν_{M-O}
H_9L^2	3430	2928	1638 1570 1470	1412 -	1290 1079 1046	896 771	667 616	544 457	-
$[Fe_2(H_7L^2)_2(H_5L^2)(H_2O)_4]6H_2O$	3408	2929	1653 1564 -	1392 1340	1295 1252 1149 1079 1011	896 854 772	666 603	456 -	541
$[Co(H_7L^2)(H_2O)_4]$	3447	-	1636 1568 -	1420 1313	1079 -	-	-	- -	608
$[Ni(H_7L^2)(H_2O)_4]2H_2O$	3435	-	1640 1566 -	1403 1315	- 1160 1080 1019	-	666 607	547 -	470
$[Cu(H_7L^2)(H_2O)_2]$	3446	-	1651 1564	1401 -	1262 1078 1012	895 778	-	- -	606 524

c) Six intense bands are appeared at 1540, 1470, 1446, 1424, 1393 and 1358 cm^{-1} in the free ligand assigned to ν_{NO2} [30]. Some of them (1470, 1446, 1424 and 1358 cm^{-1}) are unchanged during complexation, while the 1540 cm^{-1} band becomes 1525 cm^{-1}, 1393 cm^{-1} band is disappeared and a new band is appeared at 1302cm^{-1}, indicating the involving one of the nitro group in complexation.

d)The ligand gave intense bands at 1124, 1104, 1067, 1034, 1011, 980, 953, 921 and 898cm^{-1}, are assigned to the $\nu_{S=O}$. These bands are disappeared on complexation with Co(II) by coordinating through oxygen atom of the sulphonic acid group except those at 1104, 1034 980 cm^{-1} are remained.

e) The different modes of vibrations of C-C, C=C and C-H are affected on complexation, probably due to that the aromaticity of the formed chelate differs from that of the ligand.

f) The appearance of new intense band in complex in the frequency 433cm^{-1}, is assigned to ν_{M-O}.

IR spectra of Hematoxylin and its complexes:

The fundamental bands of H_5L^4 (Hematoxylin) and its complexes, Table (5),illustrated that the vibrational frequencies of coordinated functional groups (e.g. ν_{OH},$\nu_{c=c,}$ ν_{OH}) are affected with different degrees.

a) The characteristic IR bands at 3521 and 3407cm^{-1} for the free ligand assigned to the ν_{OH}, the first band (3521cm^{-1}) is disappeared in all complexes, indicating the involvement of the OH group in the complexation.

b)Four bands at 2975, 2931, 2906 and 2869cm^{-1}in the free ligand assigned to ν_{C-H} are disappeared in all the complexes, where that the aromaticity of the formed chelate differs from that of the ligand.

Table (4): Fundamental infrared bands of naphthol yellow S (L^3) and its complex

Compound	ν_{OH} of H_2O	$\nu_{C=C}\nu_{C-C}$	ν_{NO2}	$\nu_{SO}{}^{3-}\nu_{CN}$	$\nu_{S=O}$ ν_{S-O}	$\nu_{C=C}$	ν_{C-H}	ν_{Na-O}	ν_{M-O}
L^3	3432	1639 1606 1289 1223	1540 1470 1446 1424 1393 1358	1195 1166 1148	1124 1104 1067 1034 1011 980 953 921 898	863 809	774 722 689 660 631 616	588 510 473	-
CoL^3	3436	1632 1605 1217	1525 1470 1448 1425 1359 1302	1195 1167	1104 1030 982	866	747 724 628	514	433

Table (5): Fundamental infrared bands of hematoxylin(H_5L^4 .3H_2O) and its complexes

Compound	ν_{OH} of H_2O	ν_{OH}	ν_{C-H}	$\nu_{C=C}\nu_{C-C}$	ν_{C-OH} ν_{OH}	ν_{COH}	$\nu_{C=C}$	ν_{OH}	$\nu_{C=O}$	ν_{M-O}
H_5L^4 .3H_2O	3521	3407	2975 2931 2906 2869	1720 1642 1508	1478 1324	1289 1234 1085 1034	960 939 887	827 816 801	585 528 490 445 580	-
[Fe(H_3L^4)Cl(H_2O)$_3$].4H_2O	-	3459	-	1637 - -	1398	1297 1051	-	-		564
[Co(H_3L^4)(H_2O)$_4$].5H_2O		3436	-	1637 - -	1484 1336	1051 -	-	-	-	559
[Ni(H_3L^4)(H_2O)$_4$]5H_2O	-	3419	-	1635 - -	1488 1399 1317	1227 1074	-	-	-	564
[Cu(H_3L^4)(H_2O)$_2$].3H_2O	-	3436	-	1630 1569 -	1490 1383	1286 1219 1040 1078	-	-	690 576	512 454

c) The$\nu_{C=C}\nu_{C-C}$ bands are appeared in free ligand at 1720, 1642 and 1508cm^{-1}. The first band is disappeared in all the complexes due to complexation, while the second one in all the complexes undergoes shift with the range of 1630-1637cm^{-1}. The third band is appeared only in case of copper complex, while in case of iron, cobalt, nickel complexes, it's disappeared.

d)The $\nu_{C-OH}\nu_{OH}$ modes of vibrations are detected at 1478and 1324cm^{-1}in the free ligand. The first band is shifted in all the complexes within a range 1484-1490cm^{-1} except in Fe-complex, it disappeared. The second band undergoes a strong shift in all complexes with the range of 1317-1399cm^{-1}due to complexation via hydroxyl groups.

e) Theν_{COH} is detected at 1289, 1234, 1085 and 1034cm^{-1}. The first are shifted in iron and copper complexes, and is absent in cobalt and nickel complexes. The second band is shifted in copper and nickel complexes, and disappeared in iron and cobalt complexes. The third band is shifted in case of copper and nickel complexes to 1078 and 1074cm^{-1}, respectively and disappeared in other complexes. The fourth band is red shifted in all the complexes except in cobalt complex which is disappeared.

f) Different modes of vibrations of C=C, C=O and OH are affected on complexation.
g)New bands appeared in all hematoxylin complexes in the frequency range 454-564cm^{-1}, attributed to ν_{M-O}

Electronic spectral and magnetic susceptibility studies of Alloxan complexes:
a) The electronic absorption spectra of the deep brown iron–complex, [Fe(L^1) $(H_2O)_3Cl].2H_2O$], in DMSO gave two bands at 270 and 375 nm. The first band is assigned to the ($\pi\rightarrow\pi^*$) transition, while the last band assigned to CT ($t_{2g}\rightarrow\pi^*$) transition. These data pointed to the possibility of strong solute–solvent interaction. At room temperature μ_{eff} = 5.95B.M, suggests octahedral configuration in high spin state [31-34]. The molar conductivity value for complex in DMSO (1x10^{-3} mol) equals 0.002 ms/cm, where the anion exists in the inner coordination sphere. The structure of this complex is justified depending on bidentate nature of the alloxan through oxygen and nitrogen atoms with the presence of three water molecules and one chloride ion in the inner sphere, Figure 2.
b) A great deal of interest has been devoted to the study of the electronic spectra of Co^{II}, d^7, salts and complexes. The ground state of the free Co (II) ion, d^7, is ^4F and the first excited state is ^4P. In octahedral field, the ground state of Co (II) is three fold, $^4T_{1g}$, states, while in tetrahedral field; the non-degenerate $^4A_2$ state is the ground state. In an octahedral field, two spin multiplicities are identified. The high spin complexes with $^4T_{2g}$(F) ground state have the electronic configuration $(t_{2g})^5(e_g)^2$ with three unpaired electrons. The low spin complexes with ^2E_g ground state have configuration $(t_{2g})^6(e_g)^1$ with only one unpaired electron [35]. The electronic absorption spectra of the violet cobalt-complex,[Co(L^1)$(H_2O)_2$].3H_2O, in DMSO, gave two bands at 268 and 376nm, due to charge transfer transition, d-d transitions and to $^4A_2\rightarrow{}^4T_1$(P) transitions of the Td symmetry [36,37].Its room temperature μ_{eff} = 4.36 B.M verified such geometry. The postulated structure of this complex is based on bidentate nature of the alloxan through oxygen and nitrogen atoms with two water molecules in the inner sphere and other molecules in the outer sphere, Figure 2.
c) A large number of nickel complexes with coordination number from 4 to 6 are well known to give different geometries such as octahedral, tetrahedral, square planner and penta-coordinate. In cubic filed, the ^3F ground state splits to singly degenerate $^3A_2$ and triply degenerate terms $^3T_1$ and $^3T_2$. In addition, two spin-forbidden bands frequently observed at 770-909 nm due to $^3A_{2g}\rightarrow{}^1E_g$ (D) and $^3A_{2g}\rightarrow{}^1E_g$ (G) transitions.

In an octahedral field, no contribution from spin-orbit coupling is expected and the measured moments are in the range 2.8-3.3 B.M, very close to the spin-only value. Values for octahedral complexes are slightly above the spin-only that arise from slight mixing of a multiplet excited states in which spin-orbit coupling is appreciable [38]. By elongating one of the axis of an octahedral complex, the limiting structure of the complex will be a square-planar configuration. This structure automatically produces a diamagnetic nickel (II) complex. In a square-planar nickel (II) chelate, the separation of d_z^2 and d_x^2-$_y^2$ orbitals is very large according to diamagnetism. The bands may hide under the charge transfer bands [39].The square-planar complexes are characterized by no electronic transition that occurs below 1000 nm. This situation arises as a consequence of the large crystal field splitting in a square planar complex. Sometimes bands are observed below this region that is believed to be vibrational in origin. The bands located at 375 nm and 610 nm are assigned to be a typical octahedral geometry [40-43]. The presence of an additional weak bands at 710 and 760 nm, not observed with octahedral, are due to tetragonal distortion. The absence of a band near 900 nm assigns the diamagnetic property and its existence indicates that the complex is of low-spin type.

The electronic absorption spectra of the blue nickel–complex, [Ni(L^1)$(H_2O)_4$].3H_2O, in DMSO, gave different bands at 287, 398, 461nm, due to probable charge transfer (CT) transition nature and the d-d transitions, respectively. Its room temperature μ_{eff} = 4.48B.M gives an indication of the existence of octahedral configuration. Similarly bidentate chelation of the alloxan through oxygen and nitrogen atoms with the presence of four water molecules in the innersphere supported its structure, Figure 2.

The electronic absorption spectra of the green copper–complex, [Cu(L^1).2H_2O].H_2O, in DMSO, gave two bands at 266 and 358 nm. The first band is probably due to the charge transfer (CT), while the last band is mainly to d-d transitions. The μ_{eff} =1.95M.B at room temperature points to square planar geometry [44-46]. As given before, the proposed structure of this complex depends on bidentate chelation of the alloxan through oxygen and nitrogen atoms with the presence of two water molecules in the innersphere, Figure 2.

e) At room temperature, the cadmuim complex [Cd(HL^1)(H_2O)Cl].2H_2O,shows a diamagnetic behavior, indicating the square planar environment around the Cd(II) ion. The electronic spectra of Cd(II) complex display different absorption bands in DMSO, at 268, 359, 386 and 464 nm. The first band is due to π-π* transitions, while the last bands are mainly to d-d transtions. The molar conductivity value for the complex in DMSO (1x10^{-3}mol) equals to

0.003ms/cm. This confirms that the anion in complex is directly attached to the metal ion. The structure of cadmium complex proceeds in a similar manner to that of copper complex, Figure 2.

f) The electronic absorption spectrum of the green copper–nickel complex, $[CuNi(HL^1)_2Cl_2].5H_2O$, in DMSO,recorded three bands at 284, 397 and 462 nm.The first is probably due to the charge transfer (CT) nature, while the maximum bands at 397 and 462nm are assigned due to $^3A_{2g}(F)$-$^3T_{1g}$ (F) transitions. At room temperature μ_{eff}equals2.21M.B. However, the monomeric Cu- and Ni- complexes give room temperature magnetic moment values equal 1.95 and 4.48 B.M, respectively. One can suggest the presence of copper in the mixed complex to force the magnetic behavior of nickel to be diamagnetic rather than paramagnetic. The molar conductivity value for complex in DMSO ($1x10^{-3}$mol) equals to 0.001ms/cm, which indicate the presence of anion inside the coordination sphere, Figure 2.

g) The electronic absorption spectra of the green copper–cobalt complex $[CuCo(HL^1)(H_2O)_3OHCl_2]2H_2O$, in DMSO, show three bands at 267, 343 and 400 nm, due to π-π* transitions, and d-d transtions, respectively, with high spin state μ_{eff}valueof4.46 M.B. On the other hand, the data of Co- and Cu-monomeric complexes are 4.36 and 1.95 B.M, respectively. The mixed complex is nearly of magnetic moment value of that of monomeric cobalt complexes. This suggests that, the possibility of mostly Cu^{2+} is reduced to Cu^{+}. The molar conductivity value for complex in DMSO ($1x10^{-3}$mol) equals 0.001 ms/cm. This confirms that the anion in complex is directly attached to the metal inside the coordination sphere, Figure 2.

h) The electronic absorption spectra of the bluish green copper-nickel-cobalt complex $[CuNiCo(L^1)(NH_3)_4Cl_4]6H_2O$ in DMSO, exhibt two bands at 270 and 400nm, due to π-π* and d-d transtions, respectively. However, the molar conductivity value of the complex in DMSO ($1x10^{-3}$mol) equals 0.001ms/cm. The data of the mixed Cu-Co-Ni- complex (total μ_{eff} =5.03M.B) compared to the monomeric Cu- , Co- and Ni- monomeric complexes with their μ_{eff} equal (1.95, 4.36 and 4.48 B.M), respectively, where Cu^{2+} is probably reduced to Cu^{+} and predominated cobalt exists, meanwhile nickel is forced by the environmental of the other component to be diamagnetic, Figure 2.

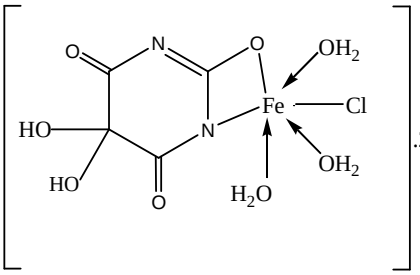

$[Fe(L^1)(H_2O)_3Cl]2H_2O$

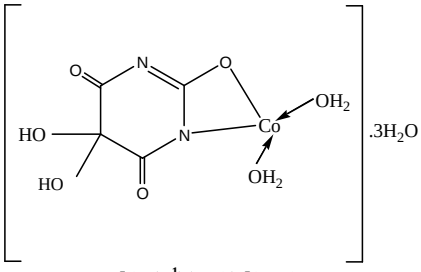

$[Co(L^1)(H_2O)_2]3H_2O$

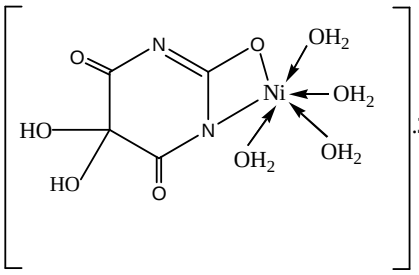

Nickel alloxan complex, $[Ni(L^1)(H_2O)_4]3H_2O$

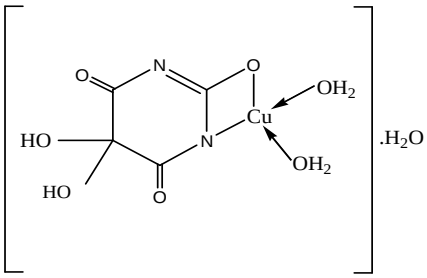

$[Cu(L^1)(H_2O)_2]H_2O$

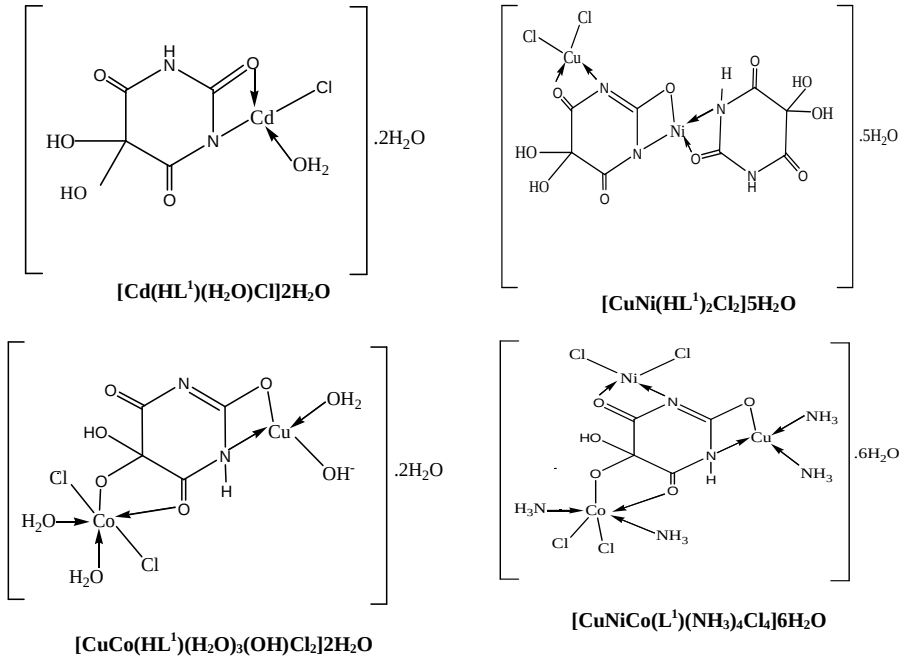

[Cd(HL^1)(H$_2$O)Cl]2H$_2$O **[CuNi(HL^1)$_2$Cl$_2$]5H$_2$O**

[CuCo(HL^1)(H$_2$O)$_3$(OH)Cl$_2$]2H$_2$O **[CuNiCo(L^1)(NH$_3$)$_4$Cl$_4$]6H$_2$O**

Figure 2. The structures of alloxan complexes

Electronic spectral and magnetic susceptibility studies of Carmine complexes:

a) The electronic absorption spectrum of the dark red iron–complex, $[Fe_2(H_7L^2)_2(H_5L^2)(H_2O)_4]6H_2O$, in ethanol, shows one band at 211nm, assigned to ($\pi\rightarrow\pi^*$) transitions. Its μ_{eff} at room temperature equals 5.93B.M, to support of O_h configuration of high spin state [31-34]. The structure of this complex is based on bidentate nature of the carmine through two oxygen atoms of OH group with four water molecules in the inner sphere, Figure 3.

b) The electronic spectral patternof the dark red cobalt-complex, $[Co(H_7L^2)(H_2O)_4]$ and violet Ni(II)-complex, $[Ni(H_7L^2)(H_2O)_4]2H_2O$, displa**y** one band at 215 ±1 nm in ethanol, assigned to charge transfer transition nature. Their magnetic momentvalues equal to4.96 and 3.12 B.M, respectively, to assign octahedral geometry around metal ion [47-50]. The structures of these complexes are based on bidentate chelation of the carmine through two oxygen atoms with existence of water four molecules in the inner sphere, Figure 3.

c) However the dark red copper complex, $[Cu(H_7L^2)(H_2O)_2]$,in ethanol, exhibits one band at 217nm, is assigned to the ($\pi\rightarrow\pi^*$) transitions. The complex has an effective room temperature magnetic value μ_{eff} (1.97B.M) of the square-planar configuration[51]. The structure complex is justified depending on bidentate nature of the carmine through two oxygen atoms with two water molecules in the innersphere, Figure 3.

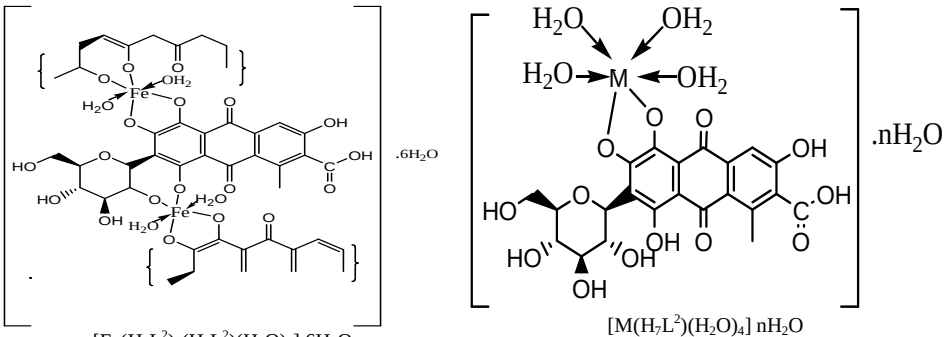

$[Fe(H_7L^2)_2(H_5L^2)(H_2O)_4].6H_2O$

$[M(H_7L^2)(H_2O)_4]\ nH_2O$

M =Co, n = 0 M =Ni, n = 2

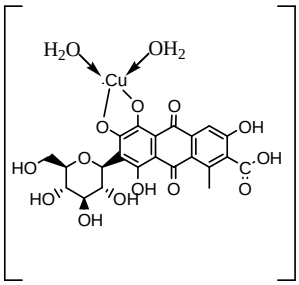

$[Cu(H_7L^2)(H_2O)_2]$

Figure 3. The structures of carmine complexes

Electronic spectral and magnetic susceptibility studies of Naphthol yellow S complex:
The green Co-complex, $[Co_2(L^3)(H_2O)_6Cl_2]2H_2O$,in ethanol, display three absorption bands at 230, 296, and 333nm, due to transitions of charge transfer, d-d transitions and of $^4T_1g(F)\rightarrow{}^4T_1g(P)$ [52] transitions, with high spin state. The μ_{eff} value of 4.95 B.M is attributed to octahedral geometry**.** The structure of complex depends on the bidentate nature of naphthol yellow S through two oxygen atoms of sulphonic group associated with two chloride atoms and two water molecules in the first site. In the second site, the metal is attached with four water molecules and two oxygen atoms, one of them from the nitro group. The molar conductivity value for complex in ethanol ($1x10^{-3}$mol) equals to 0.002 ms/cm. The molar conductance value indicates that the anion exists inside the coordination sphere, Figure 4.

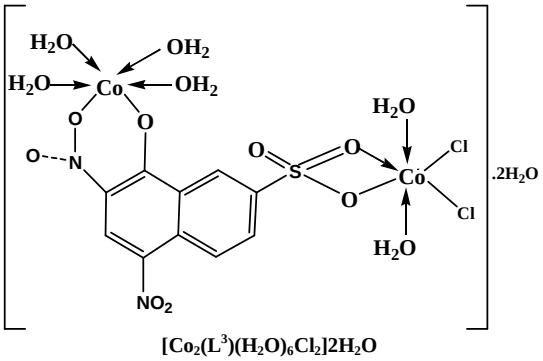

$[Co_2(L^3)(H_2O)_6Cl_2]2H_2O$

Figure 4. The structures of cobalt naphthol yellow S complex

Electronic spectral and magnetic susceptibility studies of Hematoxylin complexes:
a) The electronic spectra of black iron, cobalt and nickel complexes of hematoxylin$[Fe(H_3L^4)(H_2O)_3Cl].4H_2O$, $[Co(H_3L^4)(H_2O)_4]5H_2O$ and $[Ni(H_3L^4)(H_2O)_4]5H_2O$, respectively, exhibit three bands at (326, 400 ,463nm), (256, 287, 300nm) and (248, 325, 400nm), respectively. The bands at the 248, 256 and 287 nm are probably due to charge transfer transition, while the bands in range 300- 463 are attributed to charge transfer transition and to$^3A_2g\rightarrow{}^3T_1g$ [53]. The complex gave room temperature μ_{eff} values of 5.93M.B, 5.06M.B and 4.98 M.B, typified the existence of O_h configuration of high spine state.

The molar conductivity value for iron-complex in ethanol ($1x10^{-3}$mol) equals 0.002 ms/cm. The organic compound is of bidentate nature. The structures of these complexes are represented in Figure 5.

b)The electronic spectrum of black Cu-complex $[Cu(H_3L^4)(H_2O)_2]3H_2O$,displays four absorption bands at 250, 269, 339 and 377nm. The first two bands are probably due to charge transfer transition, while the last two′s are assigned to d-d transition in the square planer geometry. Its μ_{eff} value equals to 1.82.B.M suggesting the square planar structure. The structure of this complex is depending on the bidentate nature through oxygen atoms of -OH group and two molecules water in the inner sphere, Figure 5.

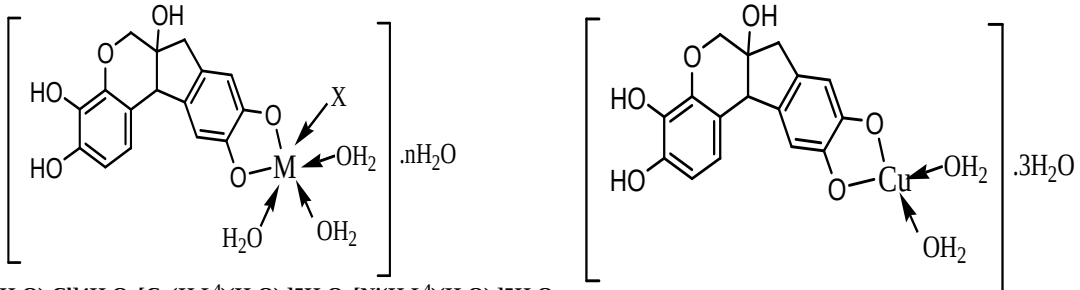

[Fe(H$_3$L^4)(H$_2$O)$_3$Cl]4H$_2$O, [Co(H$_3$L^4)(H$_2$O)$_4$]5H$_2$O, [Ni(H$_3$L^4)(H$_2$O)$_4$]5H$_2$O **[Cu(H$_3$L^4)(H$_2$O)$_2$]3H$_2$O**

Figure 5. The structures of hematoxylin complexes

Electron Spin Resonance (ESR):

The room temperature ESR of green copper alloxan complex with formula, $[Cu(L^1)(H_2O)_2].H_2O$ and black copper hematoxylin complex with formula $[Cu(H_3L^4)(H_2O)_2]3H_2O$, give well clear spectral bands. The $g_s = g_{ref} \times B_{ref}/ B_s$, where g_{ref} is constant equals 2.0036 and B_{ref} is constant equals 3322 gauss.

The calculated values of g_s for two complexes equals to 1.68 and 1.69, with A = $479.16 \times 10^{-4} cm^{-1}$ and $312.5 \times 10^{-4} cm^{-1}$, respectively. These values could be pointed to association or partial reduction for copper. Generally, Cu^{II} complexes having a lower symmetry than octahedron under a free rotation or give complexes containing grossly misaligned tetragonal axes, of magnetically dilute interaction, leading to isotropic spectral feature [54]. The corresponding equation for the isotropic A value is:

$$\alpha^2 = |A|/PK + g - 2.0023/K$$

P is the free-ion dipole term proportional to $^1/r^3$ and is given a value of $0.036 cm^{-1}$. K is the Fermi contact term and is usually given a value of o.43. If the assumption that error on using the above equation is due to a 4s contribution is correct, then this equation can be written in the form:

$$\alpha^2 = |A|/PK + g - 2.0023/K + 1 - F^2/PK$$

Based on the preceding data, the α^2 and F^2 values in copper alloxan and copper hematoxylin complexes are (0.138, 0.0154) and (0.93, 0.0154), respectively.

However, in case of rhombic dark red copper carmine complex with the formula, $[Cu(H_7L^2)(H_2O)_2]$, gave three peak at 2104.14, 3645,78 and 3979.11 gauss values with g_1, g_2 and g_3 tensor values 3.16, 1.82 and 1.67, respectively. The $g_1 > g_2 > g_3$, isdue to misalignment of local copper (II) environment. The calculated g_{av}value (2.21) is obtained from the following equation:

$$g_{av} = {}^1/_3 (g_1 + g_2 + g_3)$$

In the present case, the parameter R [55,56] is calculated from the relation $R = (g_2 - g_1 / g_3 - g_2)$. If R is > 1, a predominantly dz^2 ground state is assigned with trigonal bipyramidal geometry (TBP), while with R<1, the ground state should be dx^2-y^2 of square pyramidal geometry (SPY) [57,58].The datum of the R value of this complex typified the existence of five coordinate (TBP) geometry of dz^2 ground state, where R = 8.93 (i.e., R>1). But from the previous data of I.R. and magnetism, where the geometry of carmine copper complex is square planar while the ESR data, pointed to (TBP). So, the scope pointed to the existence of a dynamic equilibrium between the two geometries in the solid state, Figure (6). The data are collected in Table (6).

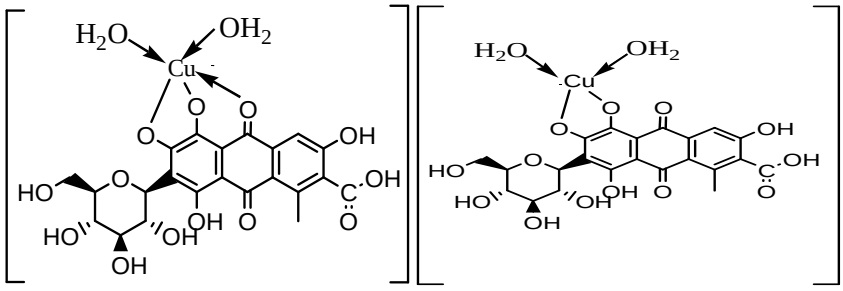

Figure 6: Proposed structures for carmine-copper complex

Table (6): ESR spectral properties for some copper complexes

Complexes	Type	g_1,($g_\parallel$)	g_2($g_\perp$)	g_3	<g>	A, ($A_\parallel$)×10^{-4} (cm^{-1})	α^2	R
$[Cu(L^1)(H_2O)_2].H_2O$	Isotropic	-	-	-	1.68	479.16	0.138	-
$[Cu(H_3L^4)(H_2O)_2\ ].3H_2O$	Isotropic				1.69	312.5	0.93	-
$[Cu(H_7L^2)(H_2O)_2]$	Rhombic	3.16	1.82	1.67	2.21	-	-	8.93

Thermal analysis studies:

The order of the thermal reaction (n) can be determined from the symmetry of the DTA curve. That is simply a/b, the reaction order and the asymmetry of the peak [59], S, are calculated as follows:

$S= 0.63\ n^2$ $n = 1.26\ (a/b)^{1/2}$

The value of the decomposed substance fraction, α_m at the moment of maximum development of reaction (with T = T_m) being determined from the relation [60].

$(1- \alpha_m) = n^{(1/\ 1-n\ )}$

The values of collision number, Z, can be obtained in case of Horowitz Metzger by making the use of the relation [61]:

$$Z = \frac{E}{RT_m}\varphi \exp\left(\frac{E}{RT_m^2}\right) = \frac{KT_m}{h}\exp\left(\frac{\Delta S^{\#}}{R}\right)$$

Where, $\Delta S^{\#}$ represents the entropy of activation, R molar gas constant, ϕ rate of heating (Ks^{-1}), K the Boltzmann constant and h the Planck's constant [62].

The heat of transformation, $\Delta H^{\#}$, can be calculated from the DTA curves [63]. In general, the change in enthalpy ($\Delta H^{\#}$) for any phase transformation-taking place at any peak temperature T_m can be given by the following equation:

$\Delta S^{\#} = \Delta H^{\#} / T_m$

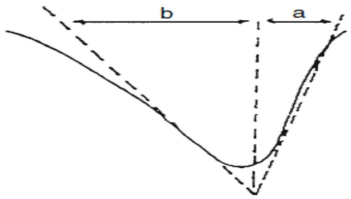

1. The thermogravimetric analysis:

a)The thermogravimetric curve for the alloxan was illustrated in the Figure7, Table 7.The first step in the temperature range 146.32 - 209.96^oC associated with mass loss (Found-11.47% / Calc-11.24 %) is due to loss of hydration water molecule [64]. The second step is within the temperature range 217.07 - 285.54^oC associated with mass loss (Found-30.33% / Calc-30.60 %) due to loss of HN and $0.5CO_2$. The third step, within temperature range 285.54 - 416.81^oC associated with mass change (Found-24.67% / Calc-23.11%) results loss of NH,O_2 and 0.5C. The

fourth degradation step within temperature range 416.81 - 599.51^{o}C with mass change (Found-32.64% / Calc-34.98%) is due to of loss two molecules of carbon monoxide.

b) The octahedral deep brown iron-complex, $[Fe(L^1)(H_2O)_3Cl]2H_2O$, Table 7, shows two successive TG peaks. The first peak is assigned to the loss of hydrated water molecules [65] at temperature range 28.5 - 113.2^{o}C, while the second step is attributed to the loss of rest coordinate water, 3CO, Cl and N_2 molecules at temperature range 113.2 - 666.9 ^{o}C. The second step is the final stage with formation iron metal oxide and C as final products.

c)The TG curve of the violet Co-complex, $[Co(L^1)(H_2O)_2]3H_2O$**,** Figure7, Table 7, shows two decomposition stages pattern within the ranges 49.75 – 267.21^{o}C and 267.21 – 561.21^{o}C, respectively, corresponding to the loss of all water molecules, and to loss of -4C, $0.5N_2$ and O_2 molecules. However, increase of temperature would lead to formation of cobalt oxide as a final product.

d) The blue nickel-complex, $[Ni(L^1)(H_2O)_4]3H_2O$**,** Table 7, indicated that the complex is thermally decomposed in five steps. The first decomposition step represents the loss of two molecules of water in the outersphere, while the second step with an estimated mass loss of (Found–6.45% / Calc6.92%) can be attributed to the liberation 1.25 water molecule. The third and fourth steps occurred within the temperature range 221.77 – 367.41^{o}C and 367.41 – 612.^{7o}C, respectively, which accounted of removal the rest of coordinated water, 4C, N_2 and $2.5O_2$ molecules. The fifth step is attributed to elimination $0.5O_2$. Further, heating would yield nickel oxide [66].

e)The TG of the pink cadmium-alloxan complex, $[Cd(HL^1)(H_2O)Cl]2H_2O$, Figure7, Table 7, starts to decompose around 48.45^{o}C. This stage continues until 120.23^{o}C and one water molecule is eliminated from outersphere [67]. The main degradation steps start at temperature range 120.23 - 297.99^{o}C and 297.99 -589.68^{o}C with overall mass loss of 62.49%. These are due to removal the rest of water molecules, N_2O, HCl and 3CO molecules. However, final product from degradation process is cadmium metal.

f) The TG curve of copper-carmine complex, $[Cu(H_7L^2)(H_2O)_2]3H_2O$, Table 7, exhibits three decomposition peaks at temperature range 21.24 - 107.35^{o}C, 107.35 - 203.99^{o}C and 203.99-433.92^{o}C, respectively. The first step is assigned to elimination of $2H_2O$ and 2OH molecules [68], while the second step is included lost 3C and CO molecule. The third step is associated with mass loss (Found-60.63% / Calc-60.34%) due to removal $-2(C_6H_6)$, ethylene, 3CO and $5.5O_2$ molecules. However, the residue from decomposition steps is attributed to copper oxide [69-71] as final products.

g) The TG curve for green cobalt-naphthol yellow S complex, Table 7, shows mass loss at temperature range 19.36 - 170.75^{o}C indicating the absence of water molecules in the complex [72]. By increasing the temperature, the TG curve of the complex exhibits a sharp drop at temperature range 170.75- 508.68^{o}C which may be due to the loss of the $C_{10}H_5N_2S + Cl_2 + 5O_2$ molecules (large part of complex) and the rest of coordinated water [44]. However, the residue from decomposition steps is attributed to cobalt (III) oxide as a final product. TG data of naphthol and its complex are indicated that the naphthol ligand is more stable than its cobalt complex.

h) The TG data of copper-hematoxylin complex $[Cu(H_3L^4)(H_2O)_2]3H_2O$, Table 7, exhibit three decomposition peaks. The first peak at temperature range 37.51-130.5^{o}C, is assigned to successive removal 3.5 of water molecules. The second peak is detected at temperature range 130.5- 335.55^{o}C, and is attributed to loss of C_6H_6, CO_2 and $1.5H_2O$. The third peak is shows at temperature range 335.55-599.93^{o}C, which is assigned to successive removal of C_6H_6 and 3CO molecules. However, the residue from degradation steps is formation of CuO.

2. Thermodynamic and kinetic studies:

To assess the influences of the structural properties of the chelating agent and the type of the metal on the thermal behavior of the complexes, the order (n) and the heat of activation E of the various decomposition stages were determined from the TG using the Coats- Redfern [73]. The rate constant is normally expressed by the Arrhenius equation:

$$k = A\exp(-\frac{E_a}{RT})$$

Where E_a is the activation energy, A is the Arrhenius pre-exponential factor which indicates how fast the reaction occurs and R is the gas constant in J mol^{-1} K. On the basis of the following equation [74-76]:

$$In(1-\alpha) = -\frac{A}{\beta}\int_{To}^{T} \exp(-\frac{E_a}{RT})dt$$

it is possible to analyze experimental data by the integral method, in order to determine the degradation kinetic parameters A, E_a.

The Coats-Redfern [73] method is as follows:

$$In[\frac{g(\alpha)}{T^2}] = In(\frac{AR}{\beta E}) - \frac{E_a}{RT}$$

Where g(α) = 1- $(1-\alpha)^{1-n}$/1-n for n ≠ 1 and g(α) = -ln(1-α) for n= 1, R is the universal gas constant. The correlation coefficient, r, was computed using the least squares method for different values of n (n=0.33, 0.5, 0.66 and 1) by plotting In [$\frac{g(\alpha)}{T^2}$] versus 1/T for the investigated metal complexes. The n-value which gave the best fit (r ≈ 1) was chosen as the order parameter for the decomposition stage of interest. The data obtained are represented in Table 7.

Table 7: Decomposition steps with the temperature range, Kinetic parameters evaluated by Coats-Redfern equation and weight loss for the compounds and their complexes

Compound	Temperature range ºC	E_a /KJmol^{-1}	A /S^{-1}	Removal species	wt. Loss	
					Found%	Calc%
$[H_2L^1]H_2O$	146.32- 209.96ºC	146.62	$4.8x10^{13}$	H_2O	11.47	11.24
	217.07 - 285.54ºC	143.74	$6.1x10^{14}$	$HN+CO_2$	30.33	30.60
	285.54 - 416.81ºC	61.44	382.93	$0.75C+O_2+NH$	24.67	23.11
	416.81 - 599.51ºC	132.18	$1.6x10^5$	2CO	32.64	34.98
	599.51 - 600ºC	----	----	No residue	0	0
$[FeL^1(H_2O)_3Cl]2H_2O$	28.5- 113.2ºC	50.38	18.47	$2.25H_2O$	12.51	12.59
	113.2- 666.9ºC	13.96	$6.2x\ 10^{-4}$	$2.75H_2O+3CO+N_2+Cl$	59.28	61.28
	666.9 - 700ºC	----	----	Fe +CO residue	27.99	26.08
$[CoL^1(H_2O)_2]3H_2O$	49.76 - 267.21ºC	27.62	0.385	$5H_2O+0.5N_2$	35.51	35.98
	267.21- 561.68ºC	50.88	501.34	$4C+0.5N_2+3.5O_2$	41.00	40.82
	561.68- 600ºC	----	----	CoO residue	23.48	23.15
$[NiL^1(H_2O)_4]3H_2O$	30.14- 140.99ºC	39.82	177.5	$2H_2O$	10.79	11.08
	140.99 - 221.77ºC	84.96	$1.8x10^5$	$1.25H_2O$	6.45	6.92
	221.77- 367.41ºC	64.68	239.4	$3.75H_2O+0.5O_2+0.5N_2$	27.76	27.55
	367.41- 612.70ºC	101.68	$1.9x10^2$	$4C+0.5N_2+O_2$	30.90	28.95
	612.70- 665.75ºC	302.63	$5.8x10^3$	$0.5O_2$	2.77	2.46
	665.75 - 700ºC	----	-----	NiO residue	23.00	23.00
$[CuL^1(H_2O)_2]H_2O$	43.13- 251.05ºC	33.08	1.48	$3H_2O+CO+1.5O_2+0.5N_2$	46.71	46.58
	251.05 - 342.30ºC	145.32	$2.3\ x10^{15}$	$2C+0.5O_2+0.5N_2$	17.66	17.86
	342.30- 509.26ºC	84.28	479.15	CO	10.92	10.87
	509.26 - 600ºC	----	----	Cu residue	24.69	24.66
$[CdHL^1H_2OCl]2H_2O$	48.45 - 120.23ºC	43.39	$1.5\ x\ 10^3$	H_2O	5.15	5.24
	120.23- 297.99ºC	42.40	9.16	$2H_2O + 0.5NO_2$	15.22	14.84
	297.99 - 598.68ºC	77.15	27.21	$4C+HCl +0.5N_2\ 3.5O_2$	47.27	45.34
	598.68 - 600ºC	----	----	Cd residue	30.34	32.77
$[H_9L^2]$	41.6 - 106ºC	64.76	$3.6x10^5$	$C_2H_2+CO+O_2$	17.36	17.46
	106- 170ºC	54.53	$2.7x10^2$	$CH_4 + 2C$	7.36	8.12
	199.2- 288.2ºC	95.36	$4.3x10^4$	$C_2H_2 + CO_2$	14.24	14.21
	288.2- 345.4ºC	152.31	$2.3x10^{10}$	$C_5H_5 + 3CO$	31.05	30.25
	345.4 - 420.1ºC	158.04	$1.3x10^9$	$CH_3+ CO + CO_2$	17.05	17.66
	420.1- 488.9ºC	159.37	$7.9x10^7$	$CH_3+ CO_2$	13.58	11.98
	488.9- 600ºC	----	-----	NO residue	0	0
$[CoH_7L^2(H_2O)_4]$	30.08 - 128.06ºC	49.48	$1.1x\ 10^4$	$4H_2O + C$	13.08	13.51
	128.06 - 328.28ºC	35.67	0.812	$C_6H_6 + 2CO_2$	27.19	26.72
	328.28 - 506.34ºC	68.59	41.51	$2C_6H_6 + 7O_2$	44.60	43.13
	506.34 - 600ºC	----	-----	CoO + CO residue	15.12	16.56
$[NiH_7L^2(H_2O)_4]2H_2O$	28.02 - 130.2ºC	64.68	$1.1x10^{-3}$	$6H_2O + 2HO$	21.89	21.60
	130.2 - 666ºC	23.52	$2.6x10^{-4}$	$C_{18}H_{16}O_8$	54.02	54.78
	666 - 700ºC	----	----	NiO + 2C +2CO residue	22.98	21.15
$[CuH_7L^2(H_2O)_2]3H_2O$	21.24 – 107.35ºC	51.87	$5.2x10^4$	$2H_2O + 2OH$	10.56	11.86
	107.35 - 203.99ºC	50.69	548.58	3C + CO	10.54	10.84
	203.99 - 433.92ºC	37.14	0.500	$2C_6H_6 + C_2H_4 + 3CO+5.5O_2$	60.63	60.34
	433.92 - 600ºC	----	----	CuO + CO residue	18.27	18.23
$[L^3]$	24.85 - 46.57C	201.19	$3x\ 10^{31}$	0.5C	1.36	1.68
	260.94 - 456.97ºC	93.02	$1.6x\ 10^3$	$5.5C + 3H +1.25Na+ SO_4$	53.87	54.38
	542.43 - 599.6ºC	329.15	$1.7x\ 10^{17}$	0.75Na	5.01	4.84
	599.6 - 600ºC	----	-----	$4C + 2NO_2 + H$ residue	39.75	39.29
$[Co_2L^3]$	19.36-170.75ºC	26.99	2.67	$1.25H_2O$	3.34	3.48

	170.75 - 508.8°C	45.22	1.02 x 10^4	$C_{10}H_4N_2SCl_2O_2 + 6.75H_2O$	71.06	70.81
	508.68 - 600°C	----	-----	Co_2O_3 residue	25.58	25.07
$[H_5L^4]3H_2O$	26.9 - 85°C	62.43	$1.2x10^7$	$2H_2O$	9.36	10.05
	85 - 185.8°C	97.77	$3.5x10^8$	H_2O	7.87	5.05
	185.8 - 312.2°C	217.66	$5.3x10^{16}$	2OH + C	11.80	12.91
	312.2- 430.7°C	71.66	356.62	C_6H_8	22.12	22.45
	430.7 - 520°C	-----	-----	$C_9H_8O_4$ residue	49.76	50.86
$[FeH_3L^4(H_2O)_3Cl]4H_2O$	40 - 140°C	39.32	147.89	$4.75H_2O$	16.02	16.51
	140 - 694°C	19.03	$1.07x10^{-3}$	C_5H_5+ 3CO + $2.25H_2O$	37.62	36.62
	694 - 700°C	----	----	$C_8H_7O_3FeCl$ residue	45.40	46.81
$[CuH_3L^4(H_2O)_2]3H_2O$	37.51- 130.5°C	51.16	$1.7x10^4$	$3.5H_2O$	13.52	13.88
	130- 355.55°C	33.58	0.373	$C_6H_6 + CO_2 + 1.5H_2O$	34.30	32.85
	355.55 - 559.93°C	51.78	0.608	C_6H_6 + 3CO	35.14	35.96
	559.93- 600°C	----	-----	CuO residue	17.02	17.52
$[CoH_3L^4(H_2O)_4]5H_2O$	34.03- 163.53°C	39.30	146.89	$6.25H_2O$	21.49	21.58
	163.53 - 337.63°C	52.63	31.53	$2.75H_2O$ + 2CO	20.27	20.24
	337.63- 544.38°C	98.85	$6.8x10^3$	$2C_6H_6 + O_2$	35.69	36.06
	544.38 - 600°C	-----	----	Co + 2CO residue	22.55	22.05

i) All decomposition stages showed a best fit for n = 1.
ii) The activation energy, E_a, increases clearly for the subsequent degradation steps revealing a high stability of the remaining part of the chelate. The highest values suggesting a high stability due to their covalent bond character[77].
iii) According to the values of the total activation energy, the thermal stability of the metal complexes with different ligands decreases in the order:-
1. For the alloxan complexes:
$[Fe(L^1)(H_2O)_3Cl].2H_2O > [Ni(L^1)(H_2O)_4]3H_2O > [Cd(HL^1)(H_2O)Cl]2H_2O > [Co(L^1)(H_2O)_2]3H_2O > [Cu(L^1)(H_2O)_2]H_2O$.
2. For the carmine complexes: $[Ni(H_7L^2)(H_2O)_4]2H_2O > [Co(H_7L^2)(H_2O)_4] > [Cu(H_7L^2)(H_2O)_2]3H_2O$.
3. For naphthol yellow S: $L^3 > [Co_2(L^3)(H_2O)_6Cl_2]2H_2O$.
4. For hematoxylin complexes: $[Fe(H_3L^4)(H_2O)_3Cl]4H_2O > [Cu(H_3L^4)(H_2O)_2]3H_2O > [Co(H_3L^4)(H_2O)_4]5H_2O$.
iv) The value of (A) parameter lies in the range 1.07 $x10^{-3}$ to 3 $x10^{31}$.

3. The differential thermal analysis:
The DTA data of organic compounds are given in Table 8. The data allow the following observations and conclusions:
a) The DTA of alloxan, Table 8 and Figure 8, gives three peaks, the first tow's are exothermic peaks at 353 and 657°K with activation energies 62.69 and 63.38 KJ/mol with orders of 1.3 and 1.2. The exothermic peak in first step is due to elimination of H_2O molecule. The third is endothermic at 489°K with activation energy 52.00 KJ/mol and order of 1.04.
b) The red carmine compound, Table 8, gives three successive DTA peaks, where the first is endothermic at 351°K with an activation energy 44.90KJ/mol and order 1.6, followed by another exothermic peaks at 577 and 729°K with activation energies 61.73and 54.54KJ/mol and orders of 1.3 and 1.6, respectively.
c) The DTA curve for naphthol yellow S, Table 8, shows an exothermic peak at 345°K with activation energy of 62.09 KJ/mol and an order of 1.5, and another endothermic peak at 704°K with activation energy and an order of 17.74 KJ/mol and 0.5, respectively.

Table 8: DTA parameters of the ligands

Compound	Type	n	α_m	slope	T_m/°K	ΔE /KJmol^{-1}	10^3Z /Sec^{-1}	$\Delta S^{\neq}$ KJK^{-1}mol^{-1}	$\Delta H^{\neq}$ KJmol^{-1}
Alloxan	Exo	1.304	0.577	-7.445	353	62.96	0.021	-0.297	-103.77
	Endo	1.047	0.554	-8.246	489	52.00	0.016	-0.302	-147.73
	Exo	1.292	0.599	-5.547	657	63.38	0.008	-0.310	-203.88
Carmine	Endo	1.551	0.536	-5.401	351	39.96	0.015	-0.300	-104.70
	Exo	1.316	0.580	-7.425	577	61.73	0.012	-0.305	-176.41
	Exo	1.626	0.539	-6.560	729	54.54	0.008	-0.310	-226.47
Naphthol yellow S	Exo	1.527	0.552	-7.468	345	62.091	0.021	-0.297	-102.51
	Endo	0.552	0.734	-2.134	704	17.746	0.003	-0.297	-0.2979
Hematoxylin	Exo	0.759	0.681	-3.352	365	27.872	0.009	-0.304	-111.22
	Endo	1.174	0.604	-10.283	429	85.492	0.023	-0.298	-127.88
	Endo	1.162	0.580	-10.488	525	87.197	0.019	-0.301	-158.18
	Exo	1.317	0.681	-15.882	609	132.042	0.026	-0.300	-182.89
Cyanine	Exo	1.693	0.532	-3.060	373	25.447	0.008	-0.305	-114.08
	Endo	0.939	0.643	-5.104	475	42.442	0.010	-0.305	-145.33

d) The differential thermal analysis curve of hematoxylin, Table 8, consists of four peaks. The first step gave an exothermic peak at 365^{o}K associated within elimination of H_2O molecules. Its activation energy and the order were evaluated at 27.87 KJ/mol and 0.7, respectively. The second exothermic peak is appeared at 609^{o}K with an activation energy 132.04 KJ/mol and order 1.3, respectively. Two endothermic peaks are shown at 429 and 525^{o}K with activation energies 85.49 and 87.19 KJ/mol, with orders of 1.17, 1.16, respectively.
e) The DTA curve for cyanine, Table 8, shows two broad peaks. An exothermic peak at 373^{o}K has activation energy 25.4KJ/mol, and order is equal to 1.6, respectively. The endothermic peak is detected at 475^{o}K associated with an activation energy 42.4KJ/mol, and an order of 0.9, respectively.
The change of entropy, $\Delta S^{\neq}$, values for all organic compounds, is nearly of the same magnitude and lie within the range of -0.29 to -0.3 KJ/K mol. So, the transition state are more ordered, the fraction appeared in the calculated order of the thermal reaction, n and the calculated values of the collision parameters, Z, showed a direct relation to E_a [78]. The values of the decomposed substance fraction α_m, at maximum development of the reaction were calculated from Coats-Redfern [73] equation. It is nearly with the same magnitude and lies within the range 0.5 - 0.7.

Based on least square calculations, the ln ΔT versus 1000/T plots for all organic compounds gave straight lines from which, the activation energies were calculated, according to the methods of Piloyan et.al [79]. The order of chemical reaction (n) was calculated via the peak symmetry method [80-83].

4. Differential Scanning Calorimetry (DSC):
Typical DSC curves obtained for iron, nickel- alloxan, copper-carmine and (iron, cobalt, copper) - hematoxylin complexes, Figure9, are done under a flow of N_2 at heating rate 10^{o}C/min in the temperature range 25-700^{o}C. It is clear that there are no glass transition temperatures (T_g) for all complexes, where the crystallization temperatures (T_c) for all complexes are at 162.94, 74.13, 96.99, 82.5, 119.03 and 117.16^{o}C [83,84] respectively, also the melting temperature (T_m) is recorded at 234.52^{o}C only to nickel- alloxan complex. However, the DSC curve for iron- alloxan complex gave very strong endothermic peak at 61.16^{o}C it is probability of adsorbed water.

The heat capacity can be determined by dividing the heat flow by the heating rate. The variation of Cp versus T can be represented using Debye model [85,86] as the following relations:

$$C_P = \alpha T^3 + \gamma T \quad , \quad \frac{C_P}{T} = \alpha T^2 + \gamma$$

Where (a) is the slop of the line and (b) is the intersection of the line with y-axis (C_p axis). (C_p) is the specific heat at constant volume, (γ) is constant equals 10^{-4} (cal/gram. mole).

By plotting C_p/T as y-axis and T^2 as x-axis we get a straight line with a slope equal α and hence the Debye temperature can be determined from α also the intersection with y-axis gives the coefficient (γ), Table 9. Figure10 represents the variation of Cp/T versus T^2 for iron-hematoxylin complex as a demonstration.

Table 9: The slopes and intercept for DSC curves of some complexes

Complex	$C_p = a\,T + b$		$C_p/T = \alpha\,T^2 + \gamma$	
	a	b	A	Γ
$[FeL^1 3H_2OCl]2H_2O$	0.139	-48.15	3×10^{-7}	-0.031
$[NiL^1 4H_2O]3H_2O$	0.066	-21.16	2×10^{-7}	-0.019
$[CuH_7L^2 2H_2O]$	-0.276	78.22	1×10^{-6}	0.087
$[FeH_3L^4 3H_2OCl]6H_2O$	0.058	-21.4	2×10^{-7}	-0.02
$[CoH_3L^4 4H_2O]5H_2O$	-0.478	155.96	2×10^{-6}	0.180
$[CuH_3L^4(H_2O)_2]3H_2O$	-0.302	98.02	1×10^{-6}	0.113

Table (10): Bond lengths, Bond angles, Dihedral angles and Charge atoms of alloxan

Bond lengths (A°)		Bond angles (°)		Dihedral angles		Charge atoms	
Atoms	Actual	Atoms	Actual	Atoms	Actual	Atoms	Charge
N(1)-C(3)	1.372	C(3)-N(1)-C(8)	125.492	C(8)-N(1)-C(3)-C(4)	0.316	N (1)	-0.242
N(1)-C(8)	1.369	H(2)-N(1)-C(3)	117.146	C(8)-N(1)-C(3)-O(10)	-179.684	H (2)	0.000
N(1)-H(2)	1.007	H(2)-N(1)-C(8)	117.363	H(2)-N(1)-C(3)-C(4)	-179	C (3)	0.342
C(3)-C(4)	1.497	N(1)-C(3)-C(4)	117.314	H(2)-N(1)-C(3)-O(10)	0	C (4)	0.149
C(3)-O(10)	1.22	N(1)-C(3)-O(10)	119.019	C(3)-N(1)-C(8)-N(6)	0	C (5)	-0.341
C(4)-C(5)	1.497	C(4)-C(3)-O(10)	123.668	C(3)-N(1)-C(8)-O(9)	-179	N (6)	0.242-
C(4)-O(12)	1.223	C(3)-C(4)-C(5)	116.73	H(2)-N(1)-C(8)-N(6)	-179.684	H (7)	0.000
C(5)-N(6)	1.371	C(3)-C(4)-O(12)	121.551	H(2)-N(1)-C(8)-O(9)	0	C (8)	0.425
C(5)-O(11)	1.22	C(5)-C(4)-O(12)	121.72	N(1)-C(3)-C(4)-C(5)	-0.547	O (9)	-0.265
N(6)-C(8)	1.369	C(4)-C(5)-N(6)	117.316	N(1)-C(3)-C(4)-O(12)	179.451	O(10)	-0.180
N(6)-H(7)	1.007	C(4)-C(5)-O(11)	123.603	O(10)-C(3)-C(4)-C(5)	179.451	O(11)	-0.180
C(8)-O(9)	1.207	N(6)-C(5)-O(11)	119.08	O(10)-C(3)-C(4)-O(12)	-0.448	O(12)	0.194-
		C(5)-N(6)-C(8)	125.499	C(3)-C(4)-C(5)-N(6)	0.316		
		C(5)-N(6)-H(7)	117.206	C(3)-C(4)-C(5)-O(11)	-179.553		
		H(7)-N(6)-C(8)	117.295	O(12)-C(4)-C(5)-N(6)	-179.684		
		N(1)-C(8)-N(6)	117.646	O(12)-C(4)-C(5)-O(11)	0.316		
		N(1)-C(8)-O(9)	121.177	C(4)-C(5)-N(6)-C(8)	0		
		N(6)-C(8)-O(9)	121.178	C(4)-C(5)-N(6)-H(7)	-179		
				O(11)-C(5)-N(6)-C(8)	-179		
				O(11)-C(5)-N(6)-H(7)	0		
				C(5)-N(6)-C(8)-N(1)	-0.316		
				C(5)-N(6)-C(8)-O(9)	180		
				H(7)-N(6)-C(8)-N(1)	179.684		
				H(7)-N(6)-C(8)-O(9)	-0.316		

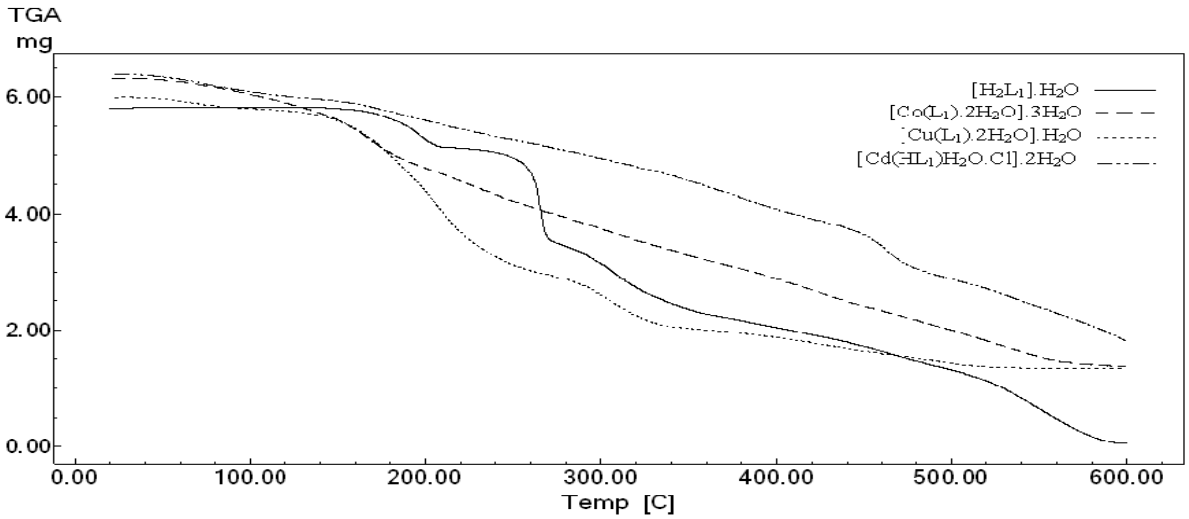

Figure 7: TGA curves for alloxan and some of its complexes

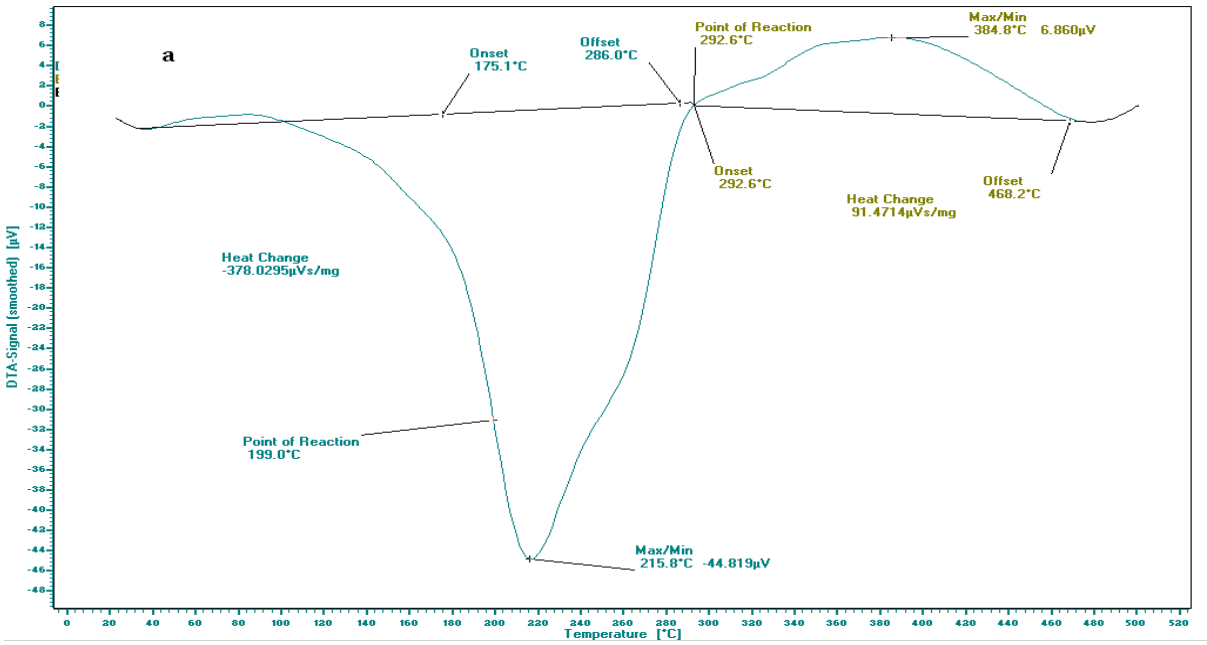

Figure 8: DTA curves for alloxan

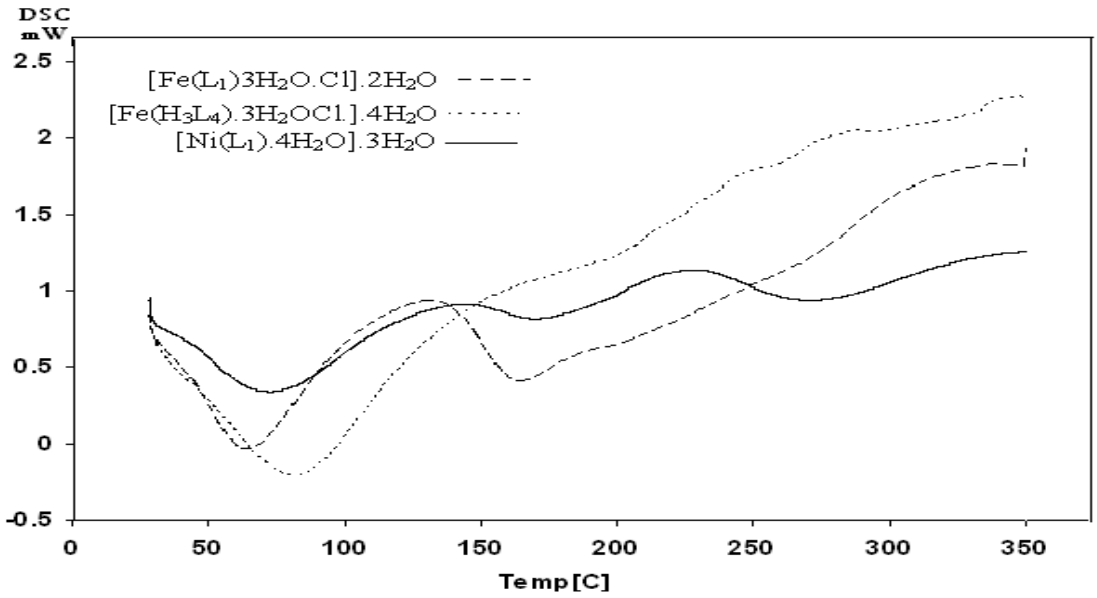

Figure 9: DSC curves for iron-, nickel-alloxan and iron-hematoxylin complexes

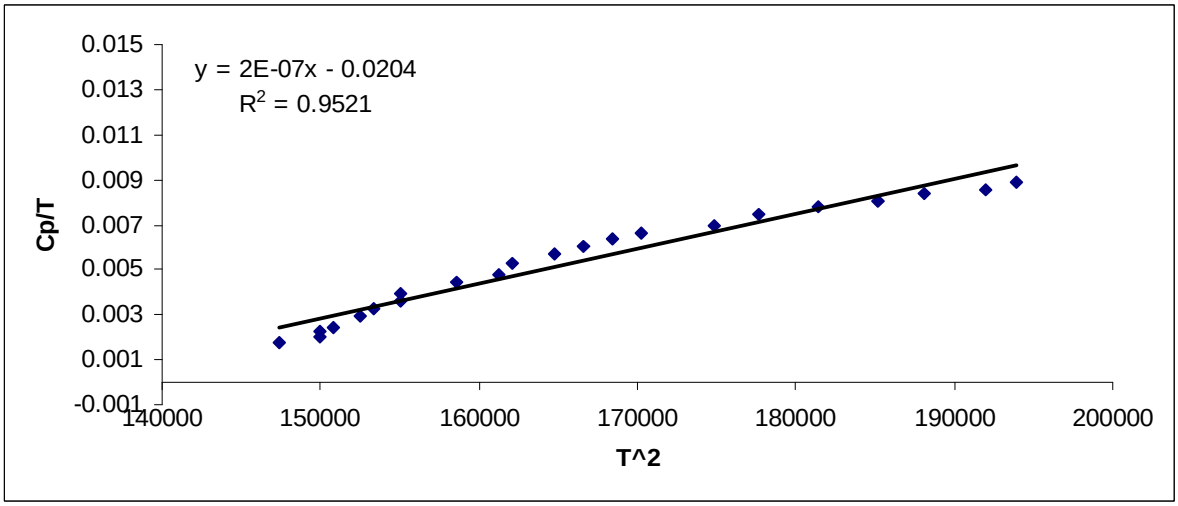

Figure10: The variation of C_p/T versus T^2 for iron-hematoxylin complex

Molecular modeling:

The molecular modeling calculations are widely increasing nowadays for the expectation of the mechanism of the reactions and the identification of the products[87]. This saves time and money. The multidentate ligands including nitrogen, sulphur and oxygen atoms are versatile and useful for assembly new molecules, because they can coordinate with many transition metal ions. Thus, the synthesis and structures of new complexes are significant for understanding the biological phenomena and exploiting artificial [88] models. Also, a theoretical support for the experimental finding regarding the donor atoms could be obtained on comparing the models of the complexes with that the free ligands.

Molecular modeling is a collective term that refers to theoretical methods and computational techniques to model the behavior of molecules[89-91]. The techniques are used in the field of computational chemistry, computational biology and materials science. The simplest calculations can be performed by hand, but inevitably computers are required to describe atoms (nucleus and electron collectively) as point charges with an associated mass. The interactions between the neighboring atoms are described by spring-like interactions (representing chemical bonds) and Van der Walls forces. The molecular modeling calculations of the free ligands (alloxan, carmine, hematoxylin, naphthol yellow S) are recorded. Figure (11) and Table (10) are given for illustration, concerning the bond lengths, bond angles, charge and dihedral angles. These calculations are based on neglecting the possibility of hydrogen bonding and using hyper chem, version 8, program.

Application of Hyper chemistry program:

According to Frontier Molecular Orbital theory (FMO) of chemical reactivity, transition of electron is due to an interaction between HOMO (highest occupied molecular orbital) and LUMO (lowest unoccupied molecular orbital) of reacting species. The energy of HOMO is directly related to the ionization potential. Higher values of E_{HOMO} indicate a tendency of the molecule to donate electron to appropriate center molecules with low energy or empty electron orbital. The energy of LUMO is directly related to the electron affinity and characterizes the susceptibility of the molecule to attack by a nucleophile. The lower values of E_{LUMO}, the stronger electron accepting abilities of the molecules. The quantum chemical parameters, χ (electronegativity), Pi (chemical potential), η(hardness) and σ(softness) were calculated [92-94]. The concepts of these parameters are related to each other, where:

$$Pi = -\chi \qquad Pi = \frac{E_{HOMO} + E_{LUMO}}{2} \qquad (Hardness)\ \eta = \frac{E_{HOMO} - E_{LUMO}}{2}$$

The inverse of the global hardness is designated as the softness (σ).

(Softness) $\sigma = \frac{1}{\eta}$

Figure (11): Molecular modeling of alloxan

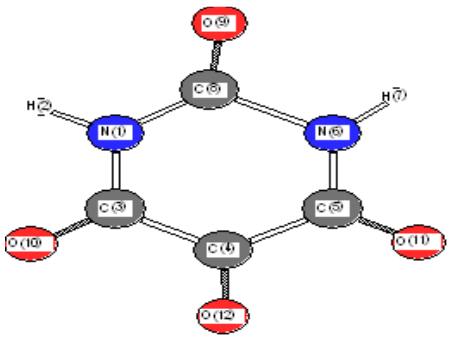

In case of alloxan, the same bond length is recorded between the following pairs of atoms, N(1)-C(3), N(1)-C(8), C(5)-N(6) and N(6)-C(8). All of them are nitrogen and carbon atoms leading to 1.37A^o, while C(3)-O(10), C(4)-O(12), C(5)-O(11) and C(8)-O(9) carbon –oxygen atoms lead to 1.2 A^o.

Table (11): The calculated quantum chemical parameters for compounds

Compound	E_{HOMO}	E_{LUMO}	ΔE	Hardness	Softness
Alloxan	-11.11	-1.74	9.37	4.68	0.21
Carmine	-9.35	-4.27	5.08	2.54	0.39
Naphthol yellow S	1.92	1.85	0.07	0.035	28.57
Hematoxylin	-9.56	-2.85	6.71	3.35	0.29

The replacement of carbon atoms by oxygen or nitrogen atoms leads to shorten the bond length due to the more electronegativity character of oxygen and nitrogen atoms. The bond angles are 117 and 121^o, the least is 116.73^o. Also, it seems that, some of dihedral angles are with ±179^o, where the distributions of the atoms are in the same plane, which occurs in case of N(1)-C(3)-C(4)-O(12), O(10)-C(3)-C(4)-C(5) and H(7)-N(6)-C(8)-N(1),the others in different planes, C(8)-N(1)-C(3)-O(10), H(2)-N(1)-C(3)-C(4), C(3)-N(1)-C(8)-O(9), H(2)-N(1)-C(8)-N(6), C(3)-C(4)-C(5)-O(11), O(12)-C(4)-C(5)-N(6), C(4)-C(5)-N(6)-H(7) and O(11)-C(5)-N(6)-C(8).

In some cases, the dihedral angles are zero. These systems are H(2)-N(1)-C(3)-O(10), C(3)-N(1)-C(8)-N(6), H(2)-N(1)-C(8)-O(9), C(4)-C(5)-N(6)-C(8) and O(11)-C(5)-N(6)-H(7). This is attributed due to the orientation and distributions of atoms are in different environments such as parallel, anti parallel leading to zero values.

The molecular modeling calculations of carmine ligand are given the following:
The same bond length is recorded between C-C and C-O atoms, where the bond lengths are 1.4, 1.5 and 1.2, 1.3 A^o, respectively. Different bond angles are recorded between atoms of carmine ligand, where the large bond angle is 133.3^o, the least is 100.79^o. Also, it seems that, some of dihedral angles are with 178±1, where the distributions of the atoms are in same plane, which occurs in the case of C(6)-C(1)-C(2)-C(26), O(21)-C(1)-C(6)-C(5), C(2)-C(1)-O(21)-H(22), C(1)-C(2)-C(3)-O(19), C(2)-C(3)-C(4)-C(7), C(3)-C(4)-C(5)-C(10), C(2)-C(26)-O(27)-C(35), C(2)-C(26)-C(28)-C(29), C(4)-C(5)-C(6)-O(17), C(8)-C(9)-C(14)-H(54), C(10)-C(9)-C(14)-C(13), C(11)-C(12)-C(13)-O(23), C(12)-C(13)-C(14)-H(54), O(23)-C(13)-C(14)-C(9), C(12)-C(13)-O(23)-H(24) and O(27)-C(35)-C(36)-O(37).

The other systems in different plane are O(21)-C(1)-C(2)-C(3), C(26)-C(2)-C(3)-C(4), O(19)-C(3)-C(4)-C(5), C(26)-O(27)-C(35)-C(36), C(10)-C(5)-C(6)-C(1), C(7)-C(8)-C(9)-C(14), C(8)-C(11)-C(12)-C(25), C(29)-C(32)-C(35)-C(36), C(25)-C(12)-C(13)-C(14), C(12)-C(25)-O(39)-H(40), H(51)-C(32)-C(35)-H(50), C(32)-C(35)-C(36)-H(45) and H(50)-C(35)-C(36)-H(46). It seems that with only one case of dihedral angel equals zero, its C(26)-C(2)-C(3)-O(19). Different environment, such parallel and anti parallel, leading to zero value.

Naphthol yellow S have different bond lengths, where O-Na is longer bond comparing withC-N**,** C-C and C-H.

In H_5L^4 (Hematoxylin), the same bond length is recorded between pairs atoms as O(1)-C(6), C(2)-C(3), C(2)-C(19), C(5)-O(26), C(8)-C(9), C(10)-C(11), C(11)-C(12) and C(19)-C(22), all of them are carbon- carbon and carbon-oxygen atoms leading to bond length equals 1.4A^o.Also , some of dihedral angles are with 178± 1, where the distribution of the atoms are in the same plane , which occurs in case of Lp(38)-O(1)-C(6)-H(30), C(3)-C(2)-C(19)-O(20), C(4)-C(3)-C(18)-C(23), C(10)-C(7)-C(8)-C(9), C(4)-C(7)-C(10)-C(11), H(35)-C(10)-C(11)-C(12), C(10)-C(11)-C(12)-O(16), O(14)-C(11)-C(12)-C(13), O(16)-C(12)-C(13)-C(8), C(11)-C(12)-O(16)-H(17), O(20)-C(19)-C(22)-C(23), and the others in different planes are O(1)-C(2)-C(3)-C(18), C(19)-C(2)-C(3)-C(4), O(1)-C(2)-C(19)-C(22), C(4)-C(7)-C(8)-C(13), C(8)-C(7)-C(10)-H(35), C(7)-C(8)-C(13)-H(32), C(9)-C(8)-C(13)-C(12), C(7)-C(10)-C(11)-O(14), C(11)-C(12)-C(13)-H(32), C(4)-C(5)-C(6)-H(31), C(3)- C(18)-C(23)-H(28), H(29)-C(18)-C(23)-C(22), C(22)-C(19)-O(20)-H(21), C(19)-C(22)-C(23)-H(28), O(24)-C(22)-C(23)-C(18), C(19)-C(22)-O(24)-H(25) .

Some systems gave zero dihedral angles. These distributions of atoms of different environments such as parallel and anti parallel leading to zero values.

The lower HOMO energy values show that molecules donating electron ability is the weaker. On contrary, the higher HOMO energy implies that the molecule is a good electron donor. LOMO energy presents the ability of a molecule receiving [94].

It was shown from, Table (11), that napththol yellow S has the smallest energy gap, so it is the soft compound compared with the other compounds. This indicates that naphthol yellow S, the more active compound to offer electrons to an acceptor (metal ions).

REFERENCES

[1] T. Szkudelski, *Physiol Res.*, **2001**, 50(6) 537-546.
[2] S.Lenzen, *Diabetologia*, **2008**, 51(2) 216-226
[3] K. Jain, J. Logothetopoulos, *Biochim. Biophys. Acta*,**1976**, 435, 145-151.
[4] R.S. Tipson, *Organic Syntheses*, *Coll*. **1963**, 4, 25; 1953, 33, 3.
[5] A. Von Zelewsky, *Inorg. Chem.*, **1981**, 20, 4448-44489.
[6] C. Daul, E. Deiss, J.N. Gex, D. Perret, D. Schaller, A. Von Zelewsky, *J. Am. Chem. Soc*., **1983**, 105, 7556-7563.
[7] R. Gupta, R.K. Saxena, P. Chatarvedi , J.S. Virdi, *J. Appl. Bacteriol*., **1995**, 78, 378-783.
[8] S.M. El-Megharbel, M.S. Refat, *Inter. J. Inno. Res. Sci. Eng. Tech.*, **2013**, 2(11) 6279-6287
[9] M.S. Refat, S.A. EL-Korashyz, D.N. Kumarx, A.S. Ahmed, J. *Coord. Chem*., **2008**, 61, 1935-1950.
[10] Z.M. Fua, H.Kosekib, Y.Iwatab, *J Loss Prevention in the Process Industries*, **2009**, 22(4) 477–483.
[11] A.H. Fischer, K.A. Jacobson, Jack Rose and Rolf Zeller, Hematoxylin and Eosin Staining of Tissue and Cell Sections, Cold Spring Harbor Laboratory Press, Cold Spring Harbor, NY, USA, **2006**.
[12] G.T. Dempsey, M. Bates, W.E. Kowtoniuk, D.R. Liu, R.Y. Tsien, and X. Zhuang, *J. Am. Chem. Soc*., **2009**,131, 18192–18193.
[13] S.J. Lord, N.R. Conley, H.L. Lee, R. Samuel, N. Liu, R.J. Twieg, W.E. Moerner, *J. Am. Chem. Soc*., **2008**, 130, 9204-9205.
[14] M. Bates, B. Huang, X. Zhuang, *Curr. Opin. Chem. Biol*., **2008**, 12, 505-514.
[15] M.S. Masoud, A.A. Soayed, A.E. Ali, O.K. Sharsherh, *J Coord. Chem.*, **2003**, 56, 725-742.
[16] M.S. Masoud, A.A. Soayed, A.E. Ali, *Spectrochim Acta*, 60A (**2004**) 1907-15.
[17] M.S. Masoud, S.S. Haggag, E.A. Khalil, *Nucleosides Nucleotides Nucleic Acids*, **2006**, 25, 73-87.
[18] M.S. Masoud, A. El-Merghany, M.Y. Abd El-Kaway,. *Synth React Inorg Met Org Nano Met Chem*, **2009**, 39, 537-553.
[19] M.S. Masoud, A. El-Merghany, A.M. Ramadan, M.Y. Abd El-Kaway, *J Therm Anal Cal*., **2010**, 101, 839-847.
[20] M.S. Masoud, A.A. Soayed, A.F. El-Husseiny, *Spectrochim Acta*, **2012**, 99A, 365-372.
[21] M.S. Masoud, M.Y. Abd El-Kaway, *Spectrochim Acta*, **2013**, 102A, 175-185.
[22] G. Schwarzenbach,"Complexometric Titration", translated by H. Irving. Methuen Co., London (**1957**).
[23] B.N. Figgis, J. Lewis, "Modern Coordination Chemistry", New York. (**1967**).
[24] M.S. Masoud, S.A. Abou- ELEnein, H.M. Kamel, *Indian J. Chem*., **2002**, 41A, 297–301.
[25] L.S. Shebaldina, O.V. Kovalchukova, S.B. Strashnova, B.E. Zaitsev, T.M. Ivanova, *Russ. J. Coord. Chem*., **2004**, 30(1) 38-42.
[26] A.J. Ivana, V.S. Zoran, S.D. Enis, M.N. Jovan, *J. Nano scale. Res. Lett*., 5 (**2010**) 81-88.
[27] D. Hadzi, *J. Chem., Soc*., (**1956**) 2725-2731.

[28] F. Billes, I.M. Ziegler, P. Bombicz, *J. Vibr. Spectro*., **2007**, 43, 193-202.
[29] I.M. Ziegler, F. Billes, *J. Molecular. Struct.*, **2002**, 618, 259-265.
[30] E. Erdem, E.Y. Sari, R. Kilincarslan , N. Kabay; *J. Trans. Met. Chem*., **2009**, 34, 167-172.
[31] E.K. Barefield, D.H. Busch, S.M. Nelson, *Quart. Rev. Chem. Soc*., **1968**, 22, 457-498.
[32] D.W. Barnum, *J. Inorg. Nucl. Chem*., **1961**, 22, 183-191.
[33] N.L. Allinger, J.C. Tai, A.M. Miller, *J. Am. Chem. Soc*., **1966**, 88, 4495-4499.
[34] M.S. Masoud, M.F. Amira, A.M. Ramadan, G.M. El-Ashry, *Spectrochim. Acta*, **2008**, 69A, 230-238.
[35] K. Jorgensen," Absorption Spectra and Chemical Bonding in Complexes", Pergamon Press, (1962).
[36] M.S. Masoud, G.B. Mohamed, Y.H. Abdul-Razek, A.E. Ali, F.N. Khairy, *J. Korean Chem. Soc*., **2002**, 46(2) 99-116.
[37] R.S. Drago, "Physical Methods in Inorganic Chemistry", Affiliated East-West Press p. VI, Ltd., New Delhi (**1979**).
[38] M.S. Masoud, A.M. Heiba, F.M. Ashmawy, *Trans. Met. Chem.*, **1983**, 8, 124-126.
[39] O. Bostrach, C.K. Jorgensen, *Acta. Chem. Scand*., 19557, 11, 1223-1231.
[40] F.A. Cotton, G. Wilkinson, "Advanced Inorganic Chemistry ", Interscience Publishing (**1996**).
[41] A.D. Leihr, C.J. Balhausen., *Annals Phys.*, **1959**, 6, 134-155.
[42] B.P. Lever, D. Ogden, *J. Chem. Soc., A*, (**1967**) 2041-2048; b) B.P. Lever, "Inorganic Electronic Spectroscopy", Elsevier Publish Co., Amsterdam (**1968**).
[43] R.Y. Parish, "The Metallic Elements", Longman Inc., New York (**1977**).
[44] E.W. Ainscough, A.M. Brodie, A.J. Dobbs, J.D. Ranford , J.M. Water, *Inorg. Chim. Acta*, **1998**, 267, 27-38.
[45] V. Ravindar, S.J. Swamy, S.S. Srihari, P. Longaiah, *Polyhedron*, **1985**, 4, 1511-1518.
[46] R. Yang, D. Wang, A. Kuang, Y. Liu, D. Jin, *Syn. React. Inorg. Metal-org. Chem*., **2001**, 31(9) 1647-1662.
[47] T.I. Kasher, A.S. EL-Tabl , R. EL-Bahnasawy, *Polish J. Chem.*, **1998**, 72, 2037-2044.
[48] K. Singh, M.S. Barwa, P. Tyagi, *Eur. J. Med. Chem.*, **2006**, 41, 147-153.
[49] A.D. Kulkarni, S.A. Patil, P.S. Badami, *Int. J. Electrochem. Sci*., **2009**, 4, 717-729.
[50] S. Chandra, M. Tyagi, K. Sharma, *J. Iran. Chem. Soc*., **2009**, 6, 310-316.
[51] J.S. Larsen, M.A. Zahran, E.B. Pedersen, C. Nielsen, *Monatsh. Chem*., **1999**, 103, 1167-1173.
[52] V.B. Rana, D.B. Singh, P. Singh, M.P. Teotia, *Trans. Met. Chem.*, **1981**, 6, 36-39.
[53] N.V. Saraf, R.D. Raut, M.D. Choudhary, *Inter. J. Sci. Res. Publ*., **2012**, 2(11) 1-5.
[54] D.R .Lorenz, J.R. Wasson, D.K. Johnson, D.A. Thorpe, *J. Inorg. Nucl. Chem*., **1975**, 37, 2297-2302.
[55] M.S. Masoud, *Metal Organic and Nano Metal Chemistry*, **2010**, 40, 1-4.
[56] J.E. Wertz, J.R. Bolton, "Electron Spin Resonace: Element Theory and Practical Applications", Chapman Hall, New York, **1986**.
[57] S. Hedeway, S.K. Hoffmann, M.S. Masoud, J. Goslar, *Spectrosc. Lett*., **1986**, 19, 917-928.
[58] M.S. Masoud, A.M. Hafez, A.E. Ali, *Spectrosc. Lett*., **1998**, 31, 901-911.
[59] H.E. Kissinger, *Anal. Chem.*, **1957**, 29, 1702-1706.
[60] H.R. Oswald, E. Dubler, Thermal Analysis, Edited by Wiedemann HG, 2, Switzerland; **1972**.
[61] H. Horowitz, G. Metzger, *Anal. Chem*., **1963**, 35, 1464-1468.
[62] M.L. Dhar, O. Singh, *J. Therm. Anal. Cal.*, **1991**, 37, 259-266.
[63] K. Traore, *J. Therm. Anal. Cal*., **1972**, 4, 135-145.
[64] G.G. Mohamed, M.A.M. Gad-Elkareem, *Spectrochim. Acta*, **2007**, 68A, 1382-1387.
[65] M. Gaber, G.B. Hefnawy, M.A. Borai, N.F. Mohamed, *J. Therm. Anal. Cal*., **2012**, 109, 1397-1405.
[66] M.N. Moreno, M.A. Romero, J.M. Salas, M.P. Sanchez, *Thermochim. Acta*, **1992**, 200, 271-280.
[67] M. Arif, S. Ur-Rehman, M. Arshad, K. Masud, N. Arshad, *Turk J Chem*, **2001**;25:73-9.
[68] M. Gaber, Y.S.Y. El-Sayed, K.Y. El-Baradie, R.M. Fahmy, *SpectrochimActa, Part A*, **2013**;107:359-70.
[69] S.L. Stefan, *J. Therm. Anal*., **1994**, 42, 1299-1312.
[70] J.P. Rski, J. Karolczyk, T. Tsumura, M. Toyoda, M. Inagaki, A.W. Morawski, *J. Therm. Anal. Cal*., **2012**, 107, 1147-1154.
[71] K.S. Rejitha, T. Ichikawa, S. Mathew, *J. Therm. Anal. Cal*., **2012**, 107, 887-892.
[72] R.L. Frost, S.J. Palmer, *J. Therm. Anal. Cal*., **2012**, 107, 901-903.
[73] A.W. Coats, J.P. Redfern, *Nature*, **1964**, 20, 68-69.
[74] T. Taakeyama, F.X. Quinn, Thermal Analysis Fundamentals and Applications to Polymer Science, John Wiley and Sons, Chichester; **1994**.
[75] J.F. Mano, D. Koniarova, R.L. Reis, *J. Mater. Sci. Mater. Med.*, **2003**, 14, 127-135.
[76] A. Broido, *J. Poly. Sci*., **1969**, 2A, 1761-1773.
[77] R.H. Abu-Eittah, M.K. Khedr, *Spectrochim. Acta*, **2009**, 71A, 1688-16894.

[78] R.C. Mackenzie, In Differential Thermal Analysis, Academic Press, London and New York; **1972**.
[79] G.O. Piloyan, I.D. Ryabchikov, O.S. Novikova, *Nature*, **1966**, 212, 1229-1229.
[80] A. Toda, C. Tomita, M. Hikosaka, Y. Saruyama Y, *Thermochim Acta*, **1998**, 324, 95-108.
[81] D.M. Ahmed, H. Saloum, M.A. El-Ries, *Thermochim. Acta*, **1990**, 159, 85-91.
[82] D.M. Ahmed, M.K. Awad, *J. Therm. Anal*., **1995**, 44, 1493-1498.
[83] R.K. Sharma, S. Mittal, M. Koel, *Crit. Rev. Anal. Chem.*, **2003**, 33, 183-197.
[84] R.K. Sharma, A. Goel, *Anal. Chim. Acta*, **2005**, 534, 137-142.
[85] S.Z.D. Cheng, Handbook of Thermal Analysis and Calorimetry, **2002**.
[86] M.S. Masoud, S.S. Haggag, A.E. Ali, N.M. Nasr, *J. Mol. Struct*., **2012**, 1014, 17-25.
[87] S. Chen, J.F. Richardson, R.M. Buchanan, *Inorg. Chem*., **1994**, 33, 2376-2382.
[88] Y. Dong, H. Fujii, M.P. Hendrish, R.A. Leising, G. Pan, C.R. Randall, E.C. Wilkinson, Y. Zang, L. Que, B.G. Fox Kauffmann, E. Munch, *J. Am. Chem. Soc.*, 1**995**, 117, 2778-2792.
[89] D. Frenkel, B. Smit, "Understanding Molecular Simulation: From Algorithms to Applications" **1996**.
[90] A.R. Leach, "Molecular Modeling: Principle and Applications" **2001**.
[91] M.S. Masoud, M.K. Awad, M.A. Shaker, M.M.T. Tahawy, *Corr. Sci*., **2010**, 52, 2387- 2396.
[92] R.G. Pearson, *Inorg. Chem*., **1988**, 27, 734-740.
[93] P. Geerlings, F. De Proft., W. Langenaeker, *Chem. Rev*., **2003**, 103, 1793-1873.
[94] S. Sagdinc, B. Koksoy, F. Kandemirli, S.H. Bayari, *J. Mol. Struct*., **2009**, 917, 63-70.